Rough stochastic volatility and applications of the rough Bergomi model

by

Türker Temel (CID: 01421814)

Department of Mathematics
Imperial College London
London SW7 2AZ
United Kingdom

Thesis submitted as part of the requirements for the award of the
MSc in Mathematics and Finance, Imperial College London, 2017-2018

Declaration

The work contained in this thesis is my own work unless otherwise stated.

Signature and date:

Türker TEMEL

09/09/2018

Acknowledgements

I would like to thank my thesis supervisor Dr. Antoine Jacquier for his time, encouragement and support. His guidance and supervision have been essential throughout this project and helped shape my thesis.

I am also deeply grateful to Mark Richardson, from Janus Henderson Investors, who accepted me as an intern and has never hesitated to help me whenever I was looking for an answer or advice. His knowledge and expertise have undoubtedly contributed to my work. I also want to express my gratitude to David Elms (Janus Henderson Investors) as it was a pleasure and an honour to work in his team.

Last but not least, I owe my deepest gratitude to my parents and family for always encouraging me, supporting me emotionally and financially, and helping me become the person I am today.

Contents

1   Introduction

With the advent of derivatives pricing in financial markets, modelling volatility has become an essential problematic for trading purposes and risk management.

In the widely used Black-Scholes model [6], introduced in 1970, implied volatility fail to capture the accurate shape of the volatility surface observed in the market. Pricing models should capture the volatility smile and skew and their empirical properties but the assumptions made in this model are not coherent with characteristics of the real market. Indeed, volatility is not deterministic and should not be modelled as such.

To respond to this inconsistency, volatility models have been improved throughout the last decades. In the recent models, not only is volatility time-dependent, but it is also described as a stochastic process, i.e. a non-deterministic process, driven by a standard Brownian motion. Among these so-called stochastic volatility models, the very popular Heston model [14] proves particularly useful as regards its tractability and its mean reversion property, recognized as a stylized fact of volatility in the sense that it never reaches zero nor does it go to infinity. The Hull-White [16], SABR [13] or Bergomi [4] models, along with the Heston model, also aim to reproduce the volatility surface. The prices resulting from these models allow a better generation of smiles but some stylized facts are still hard to reflect, particularly the persistence and clustering of volatility.

A stochastic model driven by a standard Brownian motion therefore proves not enough. Increments of a Brownian motion are independent, contrary to the behaviour of volatility and its long-range dependence. As a result, correlating the increments of the Brownian motion would seem less counter-intuitive and would justify the use of fractional Brownian motion.

Comte and Renault [8] introduced the Fractional Stochastic Volatility model, in which the volatility process is driven by a fractional Brownian motion. Gatheral, Jaisson and Rosenbaum [12] later reworked on this model to propose the Rough Fractional Stochastic Volatility (RFSV) model.

In the first part, we discuss about the various methods to generate paths of fractional Brownian motion. The two first methods having particularly high time and memory complexity, two other alternative methods are seen, in order to increase computational efficiency.

Next, we introduce the Rough Fractional Stochastic Volatility model and analyze the behaviour of volatility in this model. As the RFSV model generates volatility paths consistent with financial data, the model is used to forecast volatility.

In the following part, the pricing of derivatives is discussed under the rough Bergomi model and we study how this model generates volatility surfaces consistent with market data. A calibration method is proposed so as to find optimal parameters of the model. A discussion on the volatility skew then takes place in an attempt to adapt the simulation of volatility via an alternative kernel function. An additional test on Forward-start options is carried out in order to price them with the rBergomi model.

Finally, the dynamics of derivatives on VIX are analyzed using different approaches and are evaluated in Futures and options pricing.

2 Fractional Brownian motion

Throughout the course of this chapter, we consider a probability space $(\Omega, \mathcal{F}, (\mathcal{F}_t)_{t \geq 0}, \mathbb{P})$, where $\mathcal{F}$ is the natural filtration generated by a standard Brownian motion.

The concept of fractional Brownian motion (fBM) was formally introduced by Mandelbrot and Van Ness [19], whose representation of fBM connects the notion of Brownian motion to the fractional one using stochastic calculus. W^H denotes a fBM with Hurst parameter H and is defined, for every $t \in \mathbb{R}$, as

$$W_t^H = \frac{1}{\Gamma(H + \frac{1}{2})} \left(\int_{-\infty}^{t} |t - s|^{H - \frac{1}{2}} dW_s - \int_{-\infty}^{0} |s|^{H - \frac{1}{2}} dW_s \right) \tag{2.1}$$

where Γ is the gamma function[1] and W a two-sided standard Brownian motion[2] defined on $\mathbb{R}$.

2.1 Definition and properties

In this first part, a fBM is defined given its covariance structure, and significant properties of this process are presented. As a fBM is a Gaussian process, let us first remind this notion.

Definition 2.1. Gaussian process

A stochastic process $(X_t)_{t \in \mathbb{T}}$ in the index set $\mathbb{T}$ is Gaussian if for every finite set of indices $t_1, \ldots, t_n$ in $\mathbb{T}$, the vector $(X_{t_1}, \ldots, X_{t_n})$ is a multivariate Gaussian random variable.

However, unlike the standard Brownian motion, the increments of a fractional Brownian motion are not independent.

Definition 2.2. Fractional Brownian motion

A fractional Brownian motion (W_t^H) with Hurst parameter $H \in (0, 1)$ is a continuous Gaussian process with covariance structure

$$\text{Cov}(W_t^H, W_s^H) = \frac{1}{2} \left(t^{2H} + s^{2H} - |t - s|^{2H} \right), \ t, s \in \mathbb{R}.$$

Definition 2.3. Characterization of fractional Brownian motion

A fractional Brownian motion (W_t^H) with Hurst parameter $H \in (0, 1)$ is characterized by:

---

[1] The gamma function is defined, for complex numbers $z \in \mathbb{C}$ with a positive real part $(\text{Re}(z) > 0)$, via a convergent improper integral

$$\Gamma(z) = \int_0^\infty x^{z-1} e^{-x} dx.$$

[2] A two sided Brownian motion W, defined on $\mathbb{R}$, is a generalization of a standard Brownian motion, defined on $\mathbb{R}^+$, such that

$$W(t) = \begin{cases} W^1(t), & \text{if } t \geq 0 \\ W^2(-t), & \text{if } t < 0 \end{cases}$$

where W^1 and W^2 are two independent standard Brownian motions.

1. $W_0^H = 0$

2. W^H is Gaussian and, for every $t \geq 0$, $W_t^H \sim N(0, t^{2H})$

3. W^H has stationary increments: for any $s \in \mathbb{R}$

$$(W_{t+s}^H - W_t^H) \stackrel{\Delta}{=} W_s^H$$

4. W^H has $\mathbb{P}$-a.s. continuous trajectories

5. $\mathbb{E}(W_t^H W_s^H) = \frac{1}{2}\left(t^{2H} + s^{2H} - |t-s|^{2H}\right)$ for every $t, s \in \mathbb{R}$.

Remark 2.4. For $H = \frac{1}{2}$, the fBM is a standard Brownian motion. It is worth noticing that, in that case, $\mathbb{E}(W_t^H, W_s^H) = \min(t, s)$.

Fractional Brownian motions satisfy other important properties.

Definition 2.5. Self-similarity

A stochastic process $(X_t)_{t \geq 0}$ is said to be self-similar if, for any $c \geq 0$, there exists a function $\gamma : \mathbb{R}^+ \mapsto \mathbb{R}$ such that, for any $t \geq 0$,

$$X_{ct} \stackrel{d}{=} \gamma(c) X_t.$$

Proposition 2.6. *A fractional Brownian motion (W_t^H) with Hurst parameter $H \in (0,1)$ is a self-similar process such that, for any $c \geq 0$,*

$$W_{ct}^H \stackrel{d}{=} c^H W_t.$$

Definition 2.7. Hölder continuity

A function $h : \mathbb{R} \mapsto \mathbb{R}$ is Hölder continuous on $I \subset \mathbb{R}$ with Hölder exponent $\gamma \in (0,1)$ if

$$\limsup_{r \to 0} \frac{\displaystyle\sup_{\substack{s,t \in I \\ |s-t| < r}} |f(t) - f(s)|}{r^\gamma} < \infty. \tag{2.2}$$

The function f is said to be locally Hölder continuous if (2.2) holds on every bounded subset $I \subset \mathbb{R}$.

Proposition 2.8. *The paths of a fractional Brownian motion (W_t^H) with Hurst parameter $H \in (0,1)$ are almost surely locally $(H - \epsilon)$-Hölder continuous for $\epsilon \in (0, H)$.*

Remark 2.9. It can also be said that for every $T > 0$ and every $\epsilon \in (0, H)$, there exists a constant c such that, for $0 < s, t < T$,

$$|W_t^H - W_s^H| \leq c|t - s|^{H-\epsilon}.$$

Remark 2.10. The Mandelbrot-Van Ness representation of fBM can also be noted

$$W_t^H = C_H \left(\int_{-\infty}^0 \left(|t-s|^{H-\frac{1}{2}} - |s|^{H-\frac{1}{2}} \right) dW_s + \int_0^t (t-s)^{H-\frac{1}{2}} dW_s \right)$$

with

$$C_H = \sqrt{\frac{2H\Gamma(3/2 - H)}{\Gamma(H + 1/2)\Gamma(2 - 2H)}},$$

where Γ is the gamma function, $W = (W_t)_{t \in \mathbb{R}}$ is a two sided Brownian motion. C_H allows the covariance structure to be as defined.

Proof. For any $t \in \mathbb{R}$, using Ito's isometry,

$$\mathbb{E}\left[(W_t^H)^2\right] = (C_H)^2 \left(\int_{-\infty}^{0} \left(|t - s|^{H - \frac{1}{2}} - |s|^{H - \frac{1}{2}} \right)^2 ds + \int_0^t (t - s)^{2H-1} ds \right)$$

$$= (C_H)^2 t^{2H} \left(\int_{-\infty}^{0} \left(|1 - u|^{H - \frac{1}{2}} - |u|^{H - \frac{1}{2}} \right)^2 du + \int_0^1 (1 - u)^{2H-1} du \right).$$

To ensure that $\mathbb{E}\left[(W_t^H)^2\right] = t^{2H}$, C_H is taken to be

$$C_H = \left(\int_{-\infty}^{0} \left(|1 - u|^{H - \frac{1}{2}} - |u|^{H - \frac{1}{2}} \right)^2 du + \frac{1}{2H} \right)^{-\frac{1}{2}}.$$

As for the covariance structure

$$\mathbb{E}[|W_t^H - W_s^H|^2] = (C_H)^2 \left(\int_{-\infty}^{t} (t - u)^{H - \frac{1}{2}} dW_u - \int_{-\infty}^{s} (s - u)^{H - \frac{1}{2}} dW_u \right)$$

$$= (C_H)^2 \left(\int_{-\infty}^{t-s} (t - s - u)^{H - \frac{1}{2}} dW_u - \int_{-\infty}^{0} (-u)^{H - \frac{1}{2}} dW_u \right)$$

$$= (C_H)^2 \left(\int_{-\infty}^{0} \left[(t - s - u)^{H - \frac{1}{2}} - (-u)^{H - \frac{1}{2}} \right] dW_u + \int_0^{t-s} (t - s - u)^{H - \frac{1}{2}} dW_u \right)$$

which leads to

$$\mathbb{E}[|W_t^H - W_s^H|^2] = \mathbb{E}[|W_{t-s}^H|^2] = |t - s|^{2H}.$$

Indeed, it was seen that $(W_{t+s}^H - W_t^H) \overset{\Delta}{=} W_s^H$. As a result:

$$\mathbb{E}[W_t^H W_s^H] = \frac{1}{2} \left(\mathbb{E}[W_t^H] + \mathbb{E}[W_s^H] - \mathbb{E}[|W_t^H - W_s^H|^2] \right) = \frac{1}{2} \left(|t|^{2H} + |s|^{2H} - |t - s|^{2H} \right).$$

$\square$

Directly resulting from Gaussianity, the monofractal scaling property applies for fBM.

Proposition 2.11. *A fractional Brownian motion* (W_t^H) *has a monofractal scaling property:*

$$\mathbb{E}[|W_{t+\Delta}^H - W_t^H|^q] = \mathbb{E}[|W_\Delta|^q] = K_q \Delta^{Hq},$$

where $K_q = \int_{-\infty}^{\infty} |x|^q \frac{1}{\sqrt{2\pi}} e^{-\frac{x^2}{2}} dx.$

Remark 2.12. A fBM is neither a Markov process, nor a semi-martingale.

2.2   Volterra processes

Similarly to a standard Brownian motion, a fBM needs to be simulated in order to have a computational use. The simulation of fBM relies on Volterra processes of the form

$$V(t) = \int_0^t K(t,s)dW_s,$$

where W is a standard Brownian motion and K is a kernel function, absolutely continuous on $\mathbb{R}_+$ with respect to t and with a square integrable density K'. The representation of K in this context is

$$K(t,s) = 2H(t-s)^{H-1/2},$$

where H stands for the Hurst parameter. This assures that, as in the fBM case, $\mathbb{V}[V(t)] = t^{2H}$, where $\mathbb{V}$ stands for the variance. However, the covariance structure is a bit different. Indeed, for $0 < s < t$,

$$\mathbb{E}[V(t)V(s)] = 2Hs^{2H}\int_0^1 (1-u)^{H-1/2}(\frac{t}{s}-u)^{H-1/2}du = s^{2H}G(\frac{t}{s}),$$

where, for $x \geq 1$,

$$G(x) = \frac{2H}{H+1/2}x^{H-1/2}{}_2F_1(1, 1/2-H, H+3/2, x),$$

where ${}_2F_1$ is the Gaussian hypergeometric function.

Definition 2.13. Gaussian hypergeometric function

The Gaussian hypergeometric function ${}_2F_1$ of parameters a, b, c and variable $z \in \mathbb{R}$ is defined by the formal power series

$$_2F_1(a,b,c,z) := \sum_{k=0}^{\infty} \frac{(a)_k(b)_k}{(c)_k}\frac{z^k}{k!},$$

where $(.)_k$ is the rising factorial, defined as $(x)_0 = 1$ and, for $k \in \mathbb{N}$, as $(x)_k = x(x+1)\cdots(x+k-1)$.

Besides, another representation may be used with the Molchan-Golosov kernel K, defined for $0 < s < t$ as

$$K(t,s) = c_H \frac{1}{(t-s)^{1/2-H}} {}_2F_1\left(1/2-H, H-1/2, H+1/2, \frac{s-t}{t}\right),$$

where c_H is a constant. It is quite different from the previous kernel $K_H(t,s) = (t-s)^{H-1/2}$ but some properties may still be retrieved from this representation.

2.3   Simulation methods

2.3.1   Cholesky decomposition

Sample-paths of stationary Gaussian processes can be simulated when the covariance structure is known, which is the case for a fractional Brownian motion. The Cholesky decomposition method

of the covariance matrix allows to model such a Gaussian process.

In this part, the simulation of the fBM in the time-interval $[0, T]$ is done by discretizing the interval such that $0 = t_0 < t_1 < \cdots < t_n = T$, with step $h = \frac{T}{n}$. Note that $t_i = i \cdot h$. The covariance structure becomes, for any $i, j \in \{1, \ldots, n\}$,

$$\mathbb{E}[W_{t_i}^H W_{t_j}^H] = \frac{1}{2}\left(t_i^{2H} + t_j^{2H} - |t_i - t_j|^{2H}\right)$$

also expressed in the discretization grid as

$$\mathbb{E}[W_{t_i}^H W_{t_j}^H] = \frac{h^{2H}}{2}\left(i^{2H} + j^{2H} - |i - j|^{2H}\right).$$

The covariance matrix $\Gamma = (\Gamma_{i,j})_{i,j \in \{1,\ldots,n\}}$ with $\Gamma_{i,j} = \mathbb{E}[W_{t_i}^H W_{t_j}^H]$ for any $i, j \in \{1, \ldots, n\}$ is a symmetric, positive semi-definite matrix in $\mathbb{R}^{n \times n}$:

$$\Gamma = \begin{pmatrix} \mathbb{E}[W_{t_1}^H W_{t_1}^H] & \cdots & \mathbb{E}[W_{t_1}^H W_{t_n}^H] \\ & \ddots & \vdots \\ * & & \mathbb{E}[W_{t_n}^H W_{t_n}^H] \end{pmatrix}, \tag{2.3}$$

where $*$ indicates symmetry in the matrix. Hence the Cholesky decomposition

$$\Gamma = LL^T,$$

with $L \in \mathbb{R}^{n \times n}$ a lower triangular matrix with real and positive diagonal entries such that

$$L = \begin{pmatrix} l_{1,1} & 0 & \cdots & 0 \\ l_{2,1} & l_{2,2} & \cdots & 0 \\ \vdots & \vdots & \ddots & \vdots \\ l_{n,1} & l_{n,2} & \cdots & l_{n,n} \end{pmatrix}.$$

Remark 2.14. L is unique if Γ is positive-definite. Else, the diagonal of L may contain zero values.

Constructing a vector Z of size n drawn independently from a standard Gaussian distribution, i.e. $Z^T = (Z_1, \ldots, Z_n)$ with $(Z_i)_{i \in \{1,\ldots,n\}}$ i.i.d. with distribution $N(0, 1)$, the vector $(0, LZ)$ of size $n + 1$ yields a sample path of a fBM.

**Remark 2.15.** The computation of the Cholesky method has a complexity of $\mathcal{O}(n^3)$.

Algorithm 2.16. Simulation of fBM using the Cholesky method

1. Fix an equidistant grid $\{t_0, \cdots, t_n\}$ with step $h = \frac{T}{n}$ on $[0, T]$

2. Compute the covariance matrix Γ as defined in (2.3)

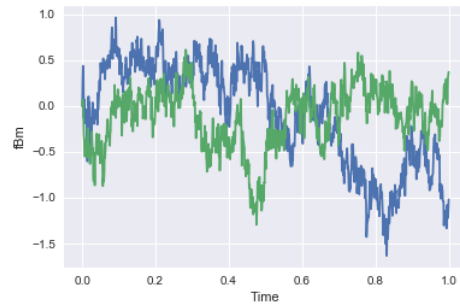3. Use the Cholesky decomposition to get L such that $\Gamma = LL^T$

4. Construct a vector Z of n independent standard normal variables

5. Return the fBM $(0, LZ)$.

On a grid of $n = 1,000$ points, the simulation of two fractional Brownian motion paths using the Cholesky decomposition gives the plots below (1).
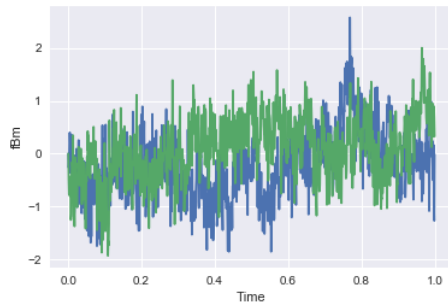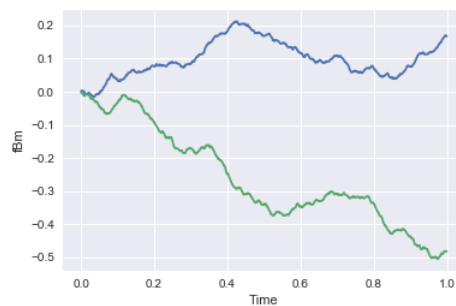

(a) $H = 0.1$

(b) $H = 0.3$

(c) $H = 0.5$

(d) $H = 0.7$

(e) $H = 0.9$

Figure 1: Simulation of fBM paths with the Cholesky method for different Hurst parameters H

2.3.2 "Circulant" Davies and Harte method

The circulant method has the same idea of finding a "square-root" of the covariance matrix. However the focus here is on the simulation of a fractional Gaussian noise, whose cumulative sums give the wanted process. Indeed, using the same time-partition as the Cholesky method, which is $0 = t_0 < t_1 < \cdots < t_n = T$, each point of the fBm can be written as

$$W_{t_i}^H = \sum_{k=1}^{i} W_{t_k}^H - W_{t_{k-1}}^H, \text{ for any } i \in \{1, \ldots, n\}.$$

The covariance matrix of a stationary discrete-time Gaussian process can be extended so as to be seen as a circulant matrix. The new matrix, if positive definite as it is for a fractional Gaussian noise, can be diagonolized using the Fast Fourier Transform (FFT) algorithm.

For any $k \in \{1, \ldots, n\}$, let the increments

$$\xi_k = W_{\frac{k}{n}}^H - W_{\frac{k-1}{n}}^H.$$

The covariance structure of these increments are represented, for any $k \in \{1, \ldots, n\}$, by

$$\rho(k) = \mathbb{E}[\xi_1 \xi_{k+1}]$$
$$= \frac{1}{2n^{2H}} \left(|k+1|^{2H} - 2|k|^{2H} + |k-1|^{2H} \right).$$

The covariance matrix is given by

$$\Gamma = \begin{pmatrix} \rho(0) & \rho(1) & \ldots & \rho(n-1) \\ \rho(1) & \rho(0) & \ldots & \rho(n-2) \\ \vdots & \vdots & \ddots & \vdots \\ \rho(n-1) & \rho(n-2) & \ldots & \rho(0) \end{pmatrix}.$$

Definition 2.17. Toeplitz matrix

A Toeplitz matrix, or diagonal-constant matrix, is a matrix in which each descending diagonal from left to right is constant.

Definition 2.18. Circulant matrix

A circulant matrix is a Toepliz matrix where each row vector is rotated one element to the right relative to the preceding row vector.

To construct a symmetric circulant matrix from the covariance matrix, we reverse the vector of $\rho(i)$ for $i \in \{1, \ldots, n-2\}$ and concatenate it with the vector of $\rho(i)$ for $i \in \{0, \ldots, n-1\}$ to use as

as the main row used in the rotation. The circulant matrix, of size $m = 2n - 2$, is represented as

$$C = \begin{pmatrix} c_0 & c_1 & \dots & c_{m-1} \\ c_{m-1} & c_0 & \dots & c_{m-2} \\ \vdots & \vdots & \ddots & \vdots \\ c_1 & c_2 & \dots & c_0 \end{pmatrix} \tag{2.4}$$

with coefficients

$$c_j = \begin{cases} \rho(j) & \text{for } j \in \{0, 1, \dots, n-2, n-1\} \\ \rho(m-j) & \text{for } j \in \{n, \dots, m-1\}. \end{cases}$$

To compute the eigenvalues of C, we first define a matrix $Q = (q_{jk})_{j,k=0}^{m-1}$ such that, for any $j, k \in \{0, \dots, m-1\}$,

$$q_{jk} = \frac{1}{\sqrt{m}} \exp\left(-2\pi i \frac{jk}{m}\right), \quad i^2 = -1.$$

The circulant matrix C can be represented as

$$C = Q\Lambda Q^*,$$

with $\Lambda = (\lambda_0, \dots, \lambda_{m-1})$ a diagonal matrix consisting of the eigenvalues of C. C is symmetric by construction, therefore the eigenvalues are real.

However, there exists an efficient method to compute the eigenvalues of C. Indeed, the expansion of Γ into the circulant matrix C makes the computation of the eigenvalues of C much more efficient using Discrete Fourier Transform (DFT). In addition, instead of choosing m as a function of n, we set m as a power of two so that computational complexity is $\mathcal{O}(n \log n)$ by applying FFT.

As a consequence,

$$C = SS^*, \text{ with } S = Q\Lambda^{1/2}Q^* \text{ and } \Lambda = (\lambda_0^{1/2}, \dots, \lambda_{m-1}^{1/2}).$$

For any $k \in \{0, \dots, m-1\}$,

$$\lambda_k = \sum_{j=0}^{m-1} c_j \exp\left(-2\pi i \frac{jk}{m}\right)$$

Therefore, the interesting simulation relies on the generation of SZ, the fractional Gaussian noise. As $SZ = Q\Lambda^{1/2}Q^*Z$, the algorithm describes the generation of the fractional Gaussian noise.

Algorithm 2.19. Simulation of fractional Gaussian noise using the Circulant method

1. Construct the circulant matrix C as defined in (2.4)

2. Apply a DFT to C to have the eigenvalues matrix Λ. As the eigenvalues are real, $\Lambda^{1/2}$, the matrix of square-root of eigenvalues, is defined.

3. Construct a vector Z of size m drawn independently from a standard Gaussian distribution

4. Apply an inverse DFT to Z to get $\sqrt{m}Q^*Z$

5. Apply a DFT to $\Lambda^{1/2}\sqrt{m}Q^*Z$ to multiply it on the left by $\frac{1}{m}Q$ so we recover SZ.

This simulation allows to generate a fractional Gaussian noise

$$SZ \sim N(0, C).$$

By taking the first n components of SZ and summing cumulatively the elements of the fractional Gaussian noise, we simulate of a path of fBM.

2.3.3 Hybrid simulation scheme

The hybrid scheme was introduced by Bennedsen, Lunde and Pakkanen [3] and is presented as a scheme simulating a Brownian semistationary process [1]. Contrary to the Cholesky method, the hybrid scheme is an approximate method but when used in rough volatility models, the results are satisfactory.

Definition 2.20. Brownian semistationary process
A Brownian semistationary process $Y = (Y_t)_{t \in \mathbb{R}}$ is (in this framework) defined by

$$Y_t = \int_{-\infty}^{t} g(t - s)\sigma(s)dW_s,$$

where W is a Brownian motion, g is a non-negative deterministic weight function on $\mathbb{R}$ and σ is a càdlàg process.

Some assumptions on the kernel function g are made so as to apply the hybrid scheme:

1. For some $\alpha \in (-\frac{1}{2}, \frac{1}{2}) \setminus \{0\}$,

$$g(x) = x^\alpha L_g(x), \quad x \in (0, 1],$$

where $L_g : (0, 1] \mapsto [0, \infty)$ is continuously differentiable, slowly varying[3] at 0 and bounded away from 0. Moreover, there exists a constant $C > 0$ such that the derivative $L_g^{'}$ or L_g satisfies

$$|L_g^{'}(x)| \leq C(1 + x^{-1}), \quad x \in (0, 1].$$

2. The function g is continuously differentiable on $(0, \infty)$.

---

[3]A measurable function $L : (0, 1] \mapsto [0, \infty)$ is slowly varying at 0 if for any $t > 0$,

$$\lim_{x \to 0} \frac{L(tx)}{L(x)} = 1.$$

3. For some $\beta \in (-\infty, -1/2)$,

$$g(x) = \mathcal{O}(x^\beta).$$

Example 2.21. These functions satisfy the assumptions above for $\alpha \in (-\frac{1}{2}, \frac{1}{2}) \setminus \{0\}$.

Gamma kernel:

$$g(x) = x^\alpha \exp(-\lambda x), \quad \lambda > 0$$

Power-law kernel:

$$g(x) = x^\alpha (1+x)^{-\gamma - \alpha}, \quad \gamma > 1/2.$$

It is important to note that, in our case, as the time index t begins at 0, we shall work with a truncated Brownian semistationary process ($\mathcal{TBSS}$) X defined by

$$X_t = \int_0^t g(t-s)\sigma(s)dW_s.$$

On the discretization grid $\{0, \frac{1}{n}, \frac{2}{n}, \ldots, \frac{\lfloor nT \rfloor}{n}\}$, assuming that σ can be taken constant on each interval of the grid, the $\mathcal{TBSS}$ is written as

$$X_t = \sum_{k=1}^{\lfloor nT \rfloor} \int_{t-\frac{k}{n}}^{t-\frac{k-1}{n}} g(t-s)\sigma(s)dW_s \simeq \sum_{k=1}^{\lfloor nT \rfloor} \sigma\left(t - \frac{k}{n}\right) \int_{t-\frac{k}{n}}^{t-\frac{k-1}{n}} g(t-s)dW_s =: X_n(t)$$

Here, two cases are considered for g.

1. For small values of k, let us say $k < \kappa$ with a given κ, g can be approximated as in the assumptions, i.e.

$$g(t-s) \approx (t-s)^\alpha L_g\left(\frac{k}{n}\right), \quad t-s \in \left[\frac{k-1}{n}, \frac{k}{n}\right].$$

2. For larger values of k, g is approximated by

$$g(t-s) \approx g\left(\frac{b_k}{n}\right),$$

with optimal b_k shown to be [1] expressed as

$$b_k^* = \left(\frac{k^{\alpha+1} - (k-1)^{\alpha+1}}{\alpha+1}\right)^{1/\alpha}, \quad k \geq \kappa + 1.$$

The $\mathcal{TBSS}$ is therefore composed of these 2 parts so it expressed as

$$X_n(t) = X_n^{(1)}(t) + X_n^{(2)}(t)$$

$$X_n^{(1)}(t) = \sum_{k=1}^{\kappa} L_g\left(\frac{k}{n}\right) \sigma\left(t - \frac{k}{n}\right) \int_{t-\frac{k}{n}}^{t-\frac{k-1}{n}} (t-s)^\alpha dW_s$$

$$X_n^{(2)}(t) = \sum_{k=\kappa+1}^{\lfloor nT \rfloor} g\left(\frac{b_k^*}{n}\right) \sigma\left(t - \frac{k}{n}\right) \left(W_{t-\frac{k-1}{n}} - W_{t-\frac{k}{n}}\right).$$

The simulation of X on the grid $\{0, \frac{1}{n}, \frac{2}{n}, \ldots, \frac{\lfloor nT \rfloor}{n}\}$ then requires simulating

$$W_{i,j}^n = \int_{\frac{i}{n}}^{\frac{i+1}{n}} \left(\frac{i+j}{n} - s\right)^\alpha dW_s, \quad j = 1, \ldots, \kappa$$

$$W_i^n = \int_{\frac{i}{n}}^{\frac{i+1}{n}} dW_s. \tag{2.5}$$

Some properties of the processes are important to note. Using Ito's isometry:

$$\mathbb{V}\left[W_i^n\right] = \frac{1}{n}$$

$$\mathbb{V}\left[W_{i,j}^n\right] = \frac{j^{2\alpha+1} - (j-1)^{2\alpha+1}}{(2\alpha+1)n^{2\alpha+1}}$$

$$\mathbb{E}\left[W_{i,j}^n W_{i,k}^n\right] = \int_0^{1/n} \left(\frac{k}{n} - u\right)^{H-1/2} \left(\frac{j}{n} - u\right)^{H-1/2} (1 - \delta_{j,k}) du,$$

$$\mathbb{E}\left[W_{i,j}^n W_j^n\right] = \frac{j^{\alpha+1} - (j-1)^{\alpha+1}}{(\alpha+1)n^{\alpha+1}} \delta_{i,j},$$

where δ stands for the Kronecker delta. Simulating a fractional Brownian motion can be seen as simulating a Volterra process such that

$$V(t) = \sqrt{2\alpha+1} \int_0^t (t-s)^\alpha dW_s.$$

The Gaussian Volterra process is a truncated Brownian semistationary process which satisfies the conditions 2.20. Indeed, letting $\tilde{V}(t) = \frac{V(t)}{\sqrt{2H}}$, and taking $g(s) = s^{H-1/2}$, $\sigma(s) = 1$ and $L_g(s) = 1$ for $s \in (0, T)$, as $\alpha = H - \frac{1}{2} \in (-\frac{1}{2}, \frac{1}{2}) \setminus \{0\}$, $\tilde{V}$ belongs to the class of truncated Brownian semistationary processes satisfying the assumptions for the hybrid scheme.

In particular, for $\kappa = 1$, the process is simulated as

$$V_n\left(\frac{i}{n}\right) = \sqrt{2\alpha+1} \left(\int_{\frac{i-1}{n}}^{\frac{i}{n}} \left(\frac{i}{n} - s\right)^\alpha dW_s + \sum_{k=2}^i \left(\frac{b_k^*}{n}\right)^\alpha \left(W_{\frac{i-(k-1)}{n}} - W_{\frac{i-k}{n}}\right)\right),$$

using the covariance structure

$$\Sigma = \begin{pmatrix} \dfrac{1}{n} & \dfrac{1}{(\alpha+1)n^{\alpha+1}} \\ * & \dfrac{1}{(2\alpha+1)n^{2\alpha+1}} \end{pmatrix}. \tag{2.6}$$

Generating a multivariate normal variable from the covariance matrix Σ yields a path of the Volterra process.

Algorithm 2.22. Simulation of fBM using the Hybrid scheme

1. Compute covariance matrix Σ from (2.6)

2. Generate a multivariate normal variable $Z = (Z_1, Z_2)^T$ with mean $(0,0)^T$ and covariance structure Σ

3. For the integral part of $V_n\left(\frac{i}{n}\right)$, as $\int_{\frac{i-1}{n}}^{\frac{i}{n}}\left(\frac{i}{n}-s\right)^{\alpha}dW_s \sim N\left(0, \frac{1}{(2\alpha+1)n^{2\alpha+1}}\right)$, estimate it using Z_2

4. For the discrete sum part, compute $\left(\frac{b_k^*}{n}\right)^{\alpha}$ for $k \in \{2, \ldots, i\}$ then compute the convolution with Z_1

5. Sum the two parts and add the factor $\sqrt{2\alpha+1}$

2.3.4 Generalised fractional operators

An extension of Donsker's approximation of Brownian motion to fractional Brownian motion and Volterra-like process is proposed by Horvath, Jacquier and Muguruza [15].

Definition 2.23. Generalised fractional operators

For any $(\alpha, \lambda) \in (-1, 1) \times (0, 1), \alpha + \lambda \in (0, 1)$, the generalised fractional operator defined on $\mathcal{C}^{\lambda}([0, 1])$ and associated to g in the space[4] $\mathcal{L}^{\alpha}$ is

$$(\mathcal{G}^{\alpha}f)(t) := \begin{cases} \int_0^t f(s)\frac{\mathrm{d}}{\mathrm{d}t}g(t-s)ds, & \text{if } \alpha \in [0, 1-\lambda), \\ \frac{\mathrm{d}}{\mathrm{d}t}\int_0^t f(s)g(t-s)ds, & \text{if } \alpha \in (-\lambda, 0). \end{cases}$$

Based on this definition, if the process Y is a strong solution to a stochastic differential equation, then, almost surely for all $t \in [0, 1]$,

$$(\mathcal{G}^{\alpha}Y)(t) = \int_0^t g(t-s)dY_s$$

Note that the first two moments of $\mathcal{G}^{\alpha}Y$ read, for all $t \in [0, 1]$,

$$\mathbb{E}(\mathcal{G}^{\alpha}Y)(t) = 0,$$

$$\mathbb{V}(\mathcal{G}^{\alpha}Y)(t) = \int_0^t g(t-s)ds.$$

An approximation of $\mathcal{G}^{\alpha}Y$ is proposed by taking $Y = W$ a Brownian motion and letting an i.i.d. sequence of centered random variables with finite moments and $\mathbb{E}[\xi_1^2] = \sigma^2$, for every $i \in \{1, \ldots, n\}$,

$$(\mathcal{G}^{\alpha}Y)(t_i) \approx \frac{1}{\sigma\sqrt{n}}\sum_{k=1}^{i}g(t_k^*)^2,$$

with $t_i = \frac{i}{n}$ and $t_k^* \in (t_{k-1}, t_k)$ an optimal point. Now, the second moment of this approximation is, for every $i \in \{0, \ldots, n\}$,

$$\mathbb{V}\left[\frac{1}{\sigma\sqrt{n}}\sum_{k=1}^{i}g(t_k^*)^2\right] = \frac{1}{n}\sum_{k=1}^{i}g\left(t_k^*\right)^2.$$

---

[4] $\mathcal{L}^{\alpha} := \{u \mapsto u^{\alpha}L(u), L \in \mathcal{C}_b^1([0, 1])\}$

Next, matching the moments of the approximating sequence with the target process on each interval (t_{k-1}, t_k), we get

$$\frac{1}{n} g\left(t_k^*\right)^2 = \int_{t_{k-1}}^{t_k} g(t-s)^2 ds,$$

$$g\left(t_k^*\right) = \sqrt{n \int_{t_{k-1}}^{t_k} g(t-s)^2 ds}.$$

In the Riemann-Liouville fractional Brownian motion case, the kernel g is expressed as $g(u) = u^{H-1/2}$, therefore replacing and integrating gives

$$(t^*)_{(t_{k-1}, t_k)}^{H-1/2} = \left(\frac{n}{2H} \left[(t-t_{k-1})^{2H} - (t-t_k)^{2H}\right]\right)^{\frac{1}{2}},$$

where $(t^*)_{(t_{k-1}, t_k)} := t_k^*$. Using the optimal point expression, the Volterra process on $[0, t]$, for $t = 1$, can be approximated as

$$\int_0^t (t-s)^{H-1/2} dW_s = \sum_{i=1}^n \int_{t_{i-1}}^{t_i} (t-s)^{H-1/2} dWs$$

$$\simeq \sum_{i=1}^n (t^*)_{(t-t_i, t-t_{i-1})}^{H-1/2} (\Delta W)_{i-1}$$

with ΔW a vector of Brownian increments such that, for any $i \in \{0, \ldots, n-1\}$,

$$(\Delta W)_i = W_{t_{i+1}} - W_{t_i} \stackrel{d}{=} \left(\frac{1}{n}\right)^{\frac{1}{2}} Z_i$$

with Z standard normal vector. Therefore the approximation becomes

$$\int_0^t (t-s)^{H-1/2} dW_s \simeq \left(\frac{1}{n}\right)^H \sum_{i=1}^n Z_{i-1} \left[\frac{i^{2H} - (i-1)^{2H}}{2H}\right]^{\frac{1}{2}}.$$

Remark 2.24. Left-point approximation

The Volterra process can easily be estimated using a left-point approximation of the kernel:

$$\int_0^t (t-s)^{H-1/2} dW_s \simeq \sum_{i=1}^n t_{i-1}^{H-1/2} \Delta W_{n-i} = \left(\frac{1}{n}\right)^H \sum_{i=1}^n (i-1)^{H-1/2} Z_{n-i}.$$

3 Rough fractional stochastic volatility models

3.1 Motivation

The notion of fractional stochastic volatility (FSV) was introduced by Comte and Renault [8] whose main idea was to replace a standard Brownian motion in volatility models by a fractional Brownian motion. Indeed, the monofractal scaling property of the increments of log-volatility (2.11) suggests that log-volatility can be driven by a fBM.

In the FSV model, the Hurst parameter satisfies $H > 1/2$, ensuring the long-memory property of volatility. Indeed, a classical stylized fact is that volatility is a long memory process. Long memory has been explained in the sense of the slow decay of the autocorrelation functions of returns, then in the sense of non-integrability of these functions and even caracterizing this slow decay as a power-law function with exponent inferior to 1.

Later on, Gatheral, Jaisson and Rosenbaum [12] demonstrate that log-volatility indeed presents persistence but not in the classical power-law sense. Studying the smoothness of volatility processes, they presented their FSV model, called Rough Fractional Stochastic Volatility model, with the Hurst exponent satisfying $H < 1/2$. The behaviour of log-volatility paths indeed lead to a representation of those as a fractional Brownian motion with Hurst index of order 0.1, making the process rougher than Brownian motion.

In the RSFV model, volatility does not exhibit long memory, but at the same time, the long memory property is questioned and the methods used to depict this property finally prove inaccurate anyway.

We focus our study, in this part and the following one, on how the RFSV model reproduces the smoothness of the volatility process and how consistent it is with the term structure of at-the-money volatility skew and volatility surfaces.

3.2 Smoothness of the volatility process

The smoothness, or more exactly the roughness of the volatility, can be characterized by the Hurst exponent of the fractional Brownian motion driven the volatility process, in the sense of Hõlder regularity (2.2).

3.2.1 Increments of log-volatility

To assess the smoothness of the volatility process, the qth sample moment of differences of log-volatility at a given lag Δ is defined, for $q \geq 0$ and $N = \lfloor \frac{T}{\Delta} \rfloor$, and on a time grid $0 = t_0 < t_1 = \Delta < \cdots < t_N = N\Delta = \lfloor T \rfloor$ of step Δ, as

$$m(q, \Delta) = \frac{1}{N} \sum_{i=1}^{N} |\log \sigma_{t_i} - \log \sigma_{t_{i-1}}|^q. \tag{3.1}$$

If the increments of the log-volatility process are assumed to be stationary, then $m(q, \Delta)$ can be seen as an estimate of

$$\mathbb{E}[|\log \sigma_\Delta - \log \sigma_0|^q],$$

using the (strong) law of large numbers. Daily spot volatility values give a value for $m(q, \Delta)$ as defined in (3.1) with a time step $\Delta = 1$. As a proxy of daily spot variance, daily realized variance estimates are used. We use historical realized variance estimates from the Oxford-Man Institute of Quantitative Finance, where the estimation of realized variance is done with trades and quotes over the trading day from open to close.

As a reminder, the annualized realized variance of a stock price process $(S_t)_{t \geq 0}$ for the period $[0, \widetilde{T}]$ on a time grid $0 = t_0 < t_1 < \cdots < t_M = \widetilde{T}$, representing for example 5-minute prices or daily close prices, is usually defined as

$$RV^{0,\widetilde{T}} := \frac{d}{M} \sum_{i=1}^{M} \log \left(\frac{S_{t_i}}{S_{t_{i-1}}} \right)^2,$$

where $d = 252$ (days). The computation of $\log m(q, \Delta)$, for any $q \geq 0$, allows to express this quantity as a linear function of $\log \Delta$. In addition, it has been recognized as a stylized fact that the distribution of the increments of log-volatility is close to Gaussian. Therefore, under the same stationary assumption as before, the information on $m(q, \Delta)$ gives

$$\mathbb{E}[|\log \sigma_\Delta - \log \sigma_0|^q] = K_q \Delta^{\zeta_q},$$

where $K_q = \int_{-\infty}^{\infty} |x|^q \frac{1}{\sqrt{2\pi}} e^{-\frac{x^2}{2}} dx$ is the qth moment of a standard normal distribution and ζ_q is the linearity coefficient of $\log m(q, \Delta)$ against $\log \Delta$.

3.2.2 Numerical results

Next, an approximation of ζ_q is given as a linear function of q so that the monofractal scaling relationship

$$\zeta_q = Hq,$$

is observed, where H will later be seen as the Hurst exponent. However empirically, for many indices, this approximation only works for a certain range of q, namely for $q \leq 2$. As our distribution is Gaussian, the first 2 moments fully describe the process, so it may explain why $q \leq 2$ seems enough and convenient. To emphasize the range of q, let us focus on 3 indices: S&P 500, FTSE 100 and Euro Stoxx 50. The straight line corresponds to the linear fit to values of ζ_q for $q \leq 2$.
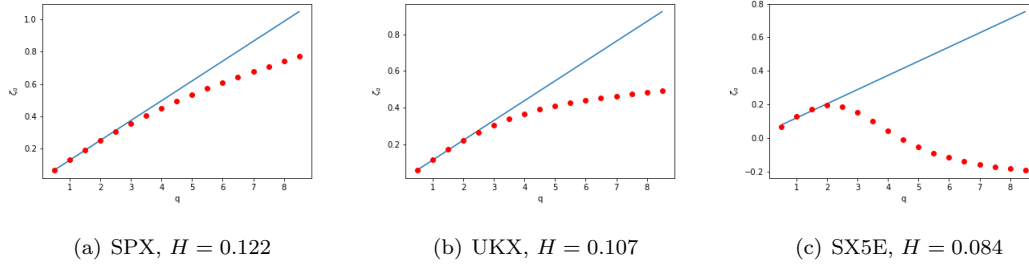

(a) SPX, $H = 0.122$ (b) UKX, $H = 0.107$ (c) SX5E, $H = 0.084$

Figure 2: Scaling of ζ_q with q

3.3   Fractional Ornstein-Uhlenbeck

On the probability space $(\Omega, \mathcal{F}, (\mathcal{F}_t)_{t \geq 0}, \mathbb{P})$, $(S_t)_{t \geq 0}$ and $(v_t)_{t \geq 0}$ are two processes that respectively model the stock price and the instantaneous variance.

The logarithm of realized variance behaves similarly as a fractional Brownian motion with Hurst exponent $H \in \left(0, \dfrac{1}{2} \right)$. The stationary RFSV model is expressed, for any $t \in [0, T]$, as

$$dS_t = \mu_t S_t \mathrm{d}t + \sigma_t S_t \mathrm{d}Zt$$

$$\sigma_t = \exp(X_t),$$

where μ is a suitable drift process, Z is a standard Brownian motion, X is a fractional Ornstein-Uhlenbeck process such that, for any $t \in \mathbb{R}$,

$$dX_t = \alpha(m - X_t)dt + \nu dW_t^H, \tag{3.2}$$

where $m \in \mathbb{R}$, $\alpha, \nu > 0$. Using the closed-form solution of an Ornstein-Uhlenbeck process, X is expressed, for any $t \in [0, T]$, as

$$X_t = m + \nu \int_{-\infty}^{t} \mathrm{e}^{-\alpha(t-s)} dW_s^H. \tag{3.3}$$

Assuming that, on the interval $[0, T]$, the rate of convergence α is "small", i.e. $\alpha << \frac{1}{T}$, the log-volatility behaves locally as a fBM.

Proposition 3.1. *As $\alpha > 0$ tends to zero,*

$$\mathbb{E}\left[\sup_{t\in[0,T]}|X_t^\alpha - X_0^\alpha - \nu W_t^H|\right] \to 0,$$

*where X^α is defined as in (3.3) and W^H is a fBM.*

Note that in the FSV model, as the Hurst parameter satisfies $H > 1/2$, α should be taken large, in the sense of $\alpha >> \frac{1}{T}$, in order to be consistent with the term structure of volatility skew. As a result, small maturities, i.e. $T << \frac{1}{\alpha}$, don't generate a proper skew.

The model generates volatility via the discretization of the fractional Ornstein-Uhlenbeck process (3.2) on an equidistant grid $\{t_0, \cdots, t_N\}$ on $[0, T]$ with step $\frac{T}{N}$ so that, for $i \in \{1, \cdots, N\}$,

$$X_{t_i} = \alpha(m - X_{t_{i-1}})(t_i - t_{i-1}) + \nu(W_{t_i}^H - W_{t_{i-1}}^H).$$

Graphically, the volatility of S&P 500 observed in the market and obtained from the model look very similar in terms of behaviour. Moreover, the volatility generated by the RFSV model is consistent with the mean reversion property of volatility, that is high (low) periods of volatility are followed by low (high) periods of volatility.
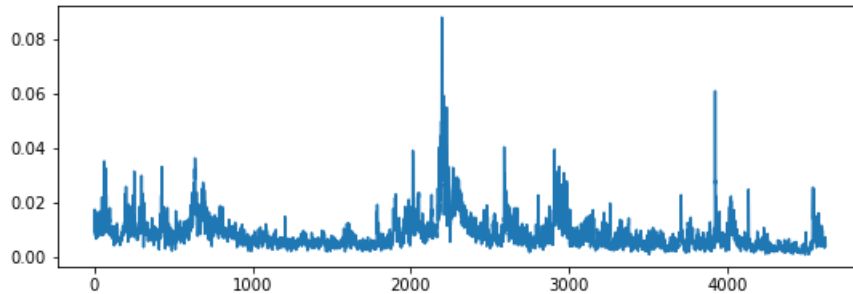
(a) Market data
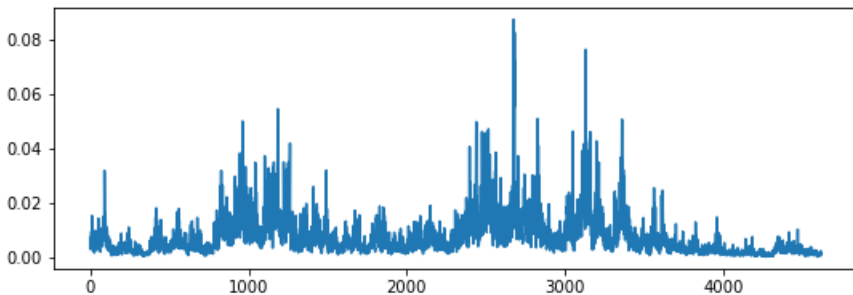
(b) RFSV model

Figure 3: Volatility of S&P 500

3.4 Variance forecast

The RFSV model allows, as a first application, to forecast log-volatility, as explained by Gatheral, Jaisson and Rosenbaum [12]. It is based on the forecast of a fBM W^H such that, for $t \in \mathbb{R}$,

$$\mathbb{E}\left[W_{t+\Delta}^H | \mathcal{F}_t\right] = \frac{\cos(H\pi)}{\pi} \Delta^{H+1/2} \int_{-\infty}^t \frac{W_s^H}{(t-s+\Delta)(t-s)^{H+1/2}} ds,$$

where $\Delta > 0$. A corollary of the proposition 3.1 is that, as α tends to zero, the increments of X^α defined in (3.2) behave as

$$\mathbb{E}[|X_{t+\Delta}^\alpha - X_t^\alpha|] \to \nu^q K_q \Delta^{qH},$$

recovering the monofractal scaling property of fBM. In the RFSV model, as the fOU volatility process is denoted by $\sigma_t = \exp(X_t)$ and as the instantaneous log-variance v behaves as a fBM with Hurst exponent H, we have

$$\log \sigma_t^2 \simeq 2\nu W_t^H + C,$$

for some constant C. The assumption that log-variance behaves as a fBM then leads to the prediction formula

$$\mathbb{E}\left[\log \sigma_{t+\Delta}^2 | \mathcal{F}_t\right] = \frac{\cos(H\pi)}{\pi} \Delta^{H+1/2} \int_{-\infty}^t \frac{\log \sigma_s^2}{(t-s+\Delta)(t-s)^{H+1/2}} ds.$$

Nuzman and Poor [21] study the conditional variance of W^H. As the process is conditionally Gaussian, given a filtration $\mathcal{F}$, one has

$$\mathbb{V}\left[W_{t+\Delta}^H | \mathcal{F}_t\right] = c\Delta^{2H},$$

where c is shown to be

$$c = \frac{\Gamma(3/2 - H)}{\Gamma(H + 1/2)\Gamma(2 - 2H)}.$$

As a result, the variance forecast formula in the RFSV model is given by

$$\mathbb{E}\left[\sigma_{t+\Delta}^2 | \mathcal{F}_t\right] = \exp\left(\mathbb{E}\left[\log \sigma_{t+\Delta}^2 | \mathcal{F}_t\right] + 2c\nu^2 \Delta^{2H}\right).$$

The simulation is carried out on the truncated interval $[0, t]$ using daily realized variance computed daily on 5-minute intervals using the previous realized variance estimates. An equidistant grid $\{0 = t_0, \cdots, t_N = t\}$ of step $\delta = \frac{t}{N}$ on $[0, t]$ is used to discretize the interval so that the integral is estimated via a left-point approximation. As a result,

$$\begin{aligned}
\int_0^t \frac{\log \sigma_s^2}{(t-s+\Delta)(t-s)^{H+1/2}} ds &= \sum_{i=1}^N \int_{t_{i-1}}^{t_i} \frac{\log \sigma_s^2}{(t-s+\Delta)(t-s)^{H+1/2}} ds \\
&\simeq \sum_{i=1}^N \frac{\log \sigma_{t_{i-1}}^2}{(t-t_{i-1}+\Delta)(t-t_{i-1})^{H+1/2}} (t_i - t_{i-1}) \qquad (3.4) \\
&= \delta \sum_{i=1}^N \frac{\log \sigma_{t_{N-i}}^2}{(t_i + \Delta)t_i^{H+1/2}}.
\end{aligned}$$

Using a rolling window scheme, each forecast is based on the data over the past 500 trading days, which approximately corresponds to 2 years, to compute historical simulation forecasts of the volatility for approximately 4000 trading days. In addition, the time is considered in days so that the interval is $\delta = 1$. Simulating results for $\mathbb{E}\left[\sigma_{t+\Delta}^2 | \mathcal{F}_t\right]$ over this horizon, the variance is annualized by multiplying the results by 252 and the volatility figures are obtained taking the square root.

As for the computation, it is quite straightforward but the computational time in this case takes a few seconds due to the large horizon of the forecasting. Moreover, our first results question the approximation in (3.4). The forecast reproduces the general shape of the observed volatility, especially the volatility spikes observed in different dates. However, there is a gap in the values observed and to tackle this problem, a modification of our approximation is necessary. Firstly, the approximation of the integral in (3.4) is based on a left-point approximation. A right-point approximation would generate a singular point $t_0 = 0$ as it would give, with $\delta = 1$,

$$\int_0^t \frac{\log \sigma_s^2}{(t - s + \Delta)(t - s)^{H+1/2}} ds \simeq \sum_{i=0}^{N-1} \frac{\log \sigma_{t_{N-i}}^2}{(t_i + \Delta)t_i^{H+1/2}}.$$

To tackle this issue, we drift a bit further from this point adding a term in ϵ so that

$$\int_0^t \frac{\log \sigma_s^2}{(t - s + \Delta)(t - s)^{H+1/2}} ds \simeq \sum_{i=0}^{N-1} \frac{\log \sigma_{t_{N-i}}^2}{(t_i + \epsilon + \Delta)(t_i + \epsilon)^{H+1/2}}.$$

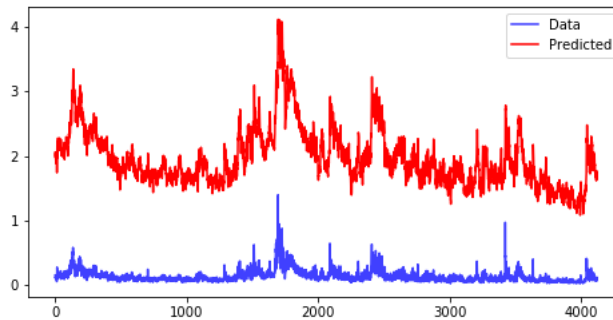We retrieve our first approximation taking $\epsilon = 1$.

Figure 4: Volatility forecast as first approximation with $\epsilon = 1$

To get closer to the singular point, we try to forecast volatility for smaller values of ϵ and the tests are done for $\epsilon \in \left\{ \dfrac{1}{4}, \dfrac{1}{2}, \dfrac{3}{4} \right\}$. The forecast with $\epsilon = 0.25$ seems, graphically, much more accurate
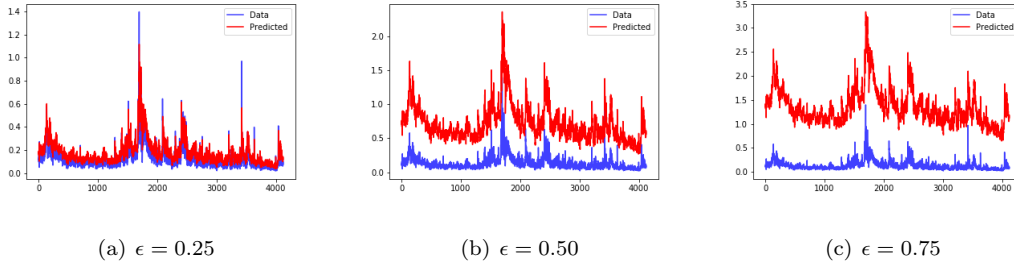

(a) $\epsilon = 0.25$ (b) $\epsilon = 0.50$ (c) $\epsilon = 0.75$

Figure 5: Volatility forecasts with different values of ϵ

hence zooming over an interval containing this point should give even better results. Now, in addition to generating forecasts for ϵ in the interval $\{0.20, 0.21, \cdots, 0.25\}$, we assess the goodness of the forecasts by computing the 2-norm of the vector containing the differences between the observed volatility σ^2 and the forecasts $\tilde{\sigma}^2$. We regroup the results in the table 1.

ϵ	0.20	0.21	0.22	0.23	0.24	0.25
$\left\| \sigma^2 - \tilde{\sigma}^2 \right\|_2^2$	15.15	12.01	10.76	11.66	14.95	20.88

Table 1: Differences between volatility and forecast

With a precision of a hundredth of unit, the difference is minimized for $\epsilon = 0.22$.
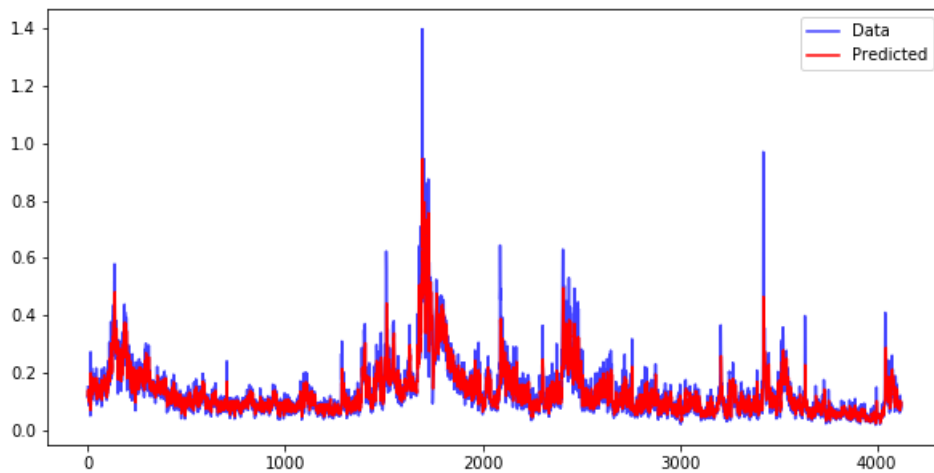

Figure 6: Volatility forecast for $\epsilon = 0.22$

4 Rough Bergomi model

Increments of log-volatility behave like a fractional Brownian motion with Hurst parameter of order 0.1 and the RFSV model with the same parameter generates volatility time series closely similar to those observed in the market.

Another instance of RFSV models is the rough Bergomi (rBergomi) model. Bayer, Friz and Gatheral [2] introduced the rBergomi model for pricing purposes on realized variance and its underlying. Simulation methods are used to generate option prices as no closed-form solution is given and the non-Markovian property resulting from the rBergomi model doesn't allow a PDE approach. Changing the pricing measure from the physical measure $\mathbb{P}$ to the pricing measure $\mathbb{Q}$, it will be seen how the rBergomi model replicates implied volatility surface dynamics accurately, with no time-dependence of the three parameters sufficient to describe the model.

4.1 Bergomi model

Instead of modelling instantaneous volatility, Bergomi has proposed in [4] to model the dynamics of forward variance. This model is known as a market model, namely a financial model consistent with market data. Indeed, the construction of the model relies on its consistency with the forward variance swap curve $\xi_t(T)$ observed at time t with maturity T. Note that the forward variance is related to a variance swap's fair strike observed at t with maturity T, denoted by $\sigma_t^2(T)$ via

$$\sigma_t^2(T) = \frac{1}{T-t} \int_t^T \xi_t(u) du,$$

or, equivalently,

$$\xi_t(T) = \frac{d}{dT}[(T-t)\sigma_t^2(T)].$$

In a general N-Brownian motions $(W^i)_{i \in \{1, \cdots, N\}}$ setting, the dynamics of $\xi_t(T)$ are described by the following SDE:

$$d\xi_t(u) = \frac{\omega}{\sqrt{\sum_{i,j=1}^N \omega_i \omega_j \rho_{i,j}}} \xi_t(u) \sum_{i=1}^N \omega_i \mathrm{e}^{-\kappa_i(u-t)} dW_t^i, \quad w, w_i, \kappa_i > 0$$

where $d[W_t^i W_t^j]_t = \rho_{i,j} dt$ for any $i, j \in \{1, \cdots, N\}$. The N-factor Bergomi variance curve model is thus expressed as

$$\xi_t(T) = \xi_0(T)\mathcal{E}\left(\sum_{i=1}^N \eta_i \int_0^t \mathrm{e}^{-\kappa_i(T-s)} dW_s^i\right),$$

where, η_i is expressed with the ω and ρ, and $\mathcal{E}$ represents the stochastic exponential[5].

---

[5]The stochastic exponential of a process $(X_t)_{t \geq 0}$ is defined as

$$\mathcal{E}(X_t) = \exp\left(X_t - X_0 - \frac{1}{2}[X]_t\right).$$

Here, we focus on a one-factor model so that the forward variance dynamics are given by

$$d\xi_t(u) = \omega(u - t)\xi_t(u)dW_t,$$

where $\omega(s) = \omega e^{-\kappa s}$, $\omega, \kappa > 0$. Applying Ito's lemma, the solution of the SDE reads, for $t > 0$,

$$\xi_t(T) = \xi_0(T) \exp\left[\omega(T - t)X_t - \frac{\omega(T-t)^2}{2}\mathbb{E}[X_t^2]\right],$$

where X is a standard Ornstein-Uhlenbeck process which satisfies

$$dX_t = -\kappa X_t dt + dW_t.$$

As a result, the Bergomi model reads

$$dS_t = r_t S_t dt + \sqrt{\xi_t(T)}S_t dW_t^{\mathbb{Q}}$$

$$d\xi_t(u) = \omega e^{-\kappa(u-t)}\xi_t(u)dZ_t^{\mathbb{Q}}, \quad \omega, \kappa > 0$$

4.2   Realized variance under $\mathbb{P}$

Using the Mandelbrot-Vann Ness representation of fractional Brownian motion in terms of Wiener integrals (2.1), increments of the logarithm of realized variance $v = \sigma^2$, under the physical measure $\mathbb{P}$, are expressed as

$$
\begin{aligned}
\log v_u - \log v_t &= 2\nu C_H \left(W_u^H - W_t^H\right) \\
&= 2\nu C_H \left(\int_{-\infty}^{u} |u - s|^{H-\frac{1}{2}}dW_s^{\mathbb{P}} - \int_{-\infty}^{t} |t - s|^{H-\frac{1}{2}}dW_s^{\mathbb{P}}\right) \\
&= 2\nu C_H \left(\int_{t}^{u} |u - s|^{H-\frac{1}{2}}dW_s^{\mathbb{P}} + \int_{-\infty}^{t} \left[|u - s|^{H-\frac{1}{2}} - |t - s|^{H-\frac{1}{2}}\right] dW_s^{\mathbb{P}}\right) \\
&=: 2\nu C_H \left[M_t(u) + Z_t(u)\right]
\end{aligned}
$$

In this expression, the left integral $M_t(u)$ is independent of $\mathcal{F}_t$ and the right integral $Z_t(u)$ is $\mathcal{F}_t$-measurable. Note that $\tilde{W}^{\mathbb{P}}$, defined as

$$\tilde{W}_t^{\mathbb{P}}(u) := \sqrt{2H}\int_{t}^{u} |u - s|^{H-\frac{1}{2}}dW_s^{\mathbb{P}} = \sqrt{2H}M_t(u)$$

has the same properties as $M_t(u)$ and let $\eta = \frac{2\nu C_H}{\sqrt{2H}}$ so that the model is written as

$$\log v_u - \log v_t = \eta\tilde{W}_t^{\mathbb{P}}(u) + 2\nu C_H Z_t(u),$$

which gives

$$v_u = v_t \exp\left(\eta\tilde{W}_t^{\mathbb{P}}(u) + 2\nu C_H Z_t(u)\right).$$

By Gaussianity, the first and second moments of $\tilde{W}_t^{\mathbb{P}}$ give $\tilde{W}_t^{\mathbb{P}}(u) \sim N\left(0, (u-t)^{2H}\right)$, which entails that $v_u|\mathcal{F}_t$ is log-normal and

$$\mathbb{E}^{\mathbb{P}}[v_u|\mathcal{F}_t] = v_t \exp\left(2\nu C_H Z_t(u) + \frac{1}{2}\eta^2(u-t)^{2H}\right).$$

In addition, in terms of stochastic exponential, the realized variance is expressed as

$$v_u = \mathbb{E}^{\mathbb{P}}[v_u|\mathcal{F}_t]\mathcal{E}\left(\eta\tilde{W}_t^{\mathbb{P}}(u)\right). \tag{4.1}$$

4.3   Change of measure

Under the physical probability measure $\mathbb{P}$, the pricing model is

$$\begin{aligned}
dS_u &= \mu_u S_u du + \sqrt{v_u}S_u dZ_u^{\mathbb{P}} \\
v_u &= v_t \exp\left(\eta\tilde{W}_t^{\mathbb{P}}(u) + 2\nu C_H Z_t(u)\right)
\end{aligned} \tag{4.2}$$

with $d[Z^{\mathbb{P}}, W^{\mathbb{P}}]_t = \rho dt$. As in the Black-Scholes framework, the pricing of options is made under an equivalent martingale measure[6] $\mathbb{Q} \sim \mathbb{P}$ on $[t, T]$:

$$dZ_u^{\mathbb{Q}} = \frac{\mu_u}{\sqrt{v_u}}du + dZ_u^{\mathbb{P}}, \tag{4.3}$$

obtained by a Girsanov change of measure on $[t, T]$ from $\mathbb{P}$ to $\mathbb{Q}$. In addition, the Brownian motion $W^{\mathbb{P}}$, which is used to construct the Volterra-type process $\tilde{W}_t^{\mathbb{P}}$, is correlated with $Z^{\mathbb{P}}$ with correlation factor ρ, empirically negative, such that

$$dW^{\mathbb{P}} = \rho dZ^{\mathbb{P}} + \sqrt{1-\rho^2}d(Z^{\perp})^{\mathbb{P}},$$

where $Z^{\perp}$ is independent of Z. Similarly to $Z^{\mathbb{P}}$, a change of measure for $(Z^{\perp})^{\mathbb{P}}$ would be of the form

$$d(Z^{\perp})_u^{\mathbb{Q}} = d(Z^{\perp})_u^{\mathbb{P}} + \gamma_u du, \tag{4.4}$$

where γ is a suitable process on $[t, T]$ seen as the market price of volatility risk. Combining (4.3) and (4.4), W can be expressed as

$$\begin{aligned}
dW^{\mathbb{Q}} &= \rho dZ^{\mathbb{Q}} + \sqrt{1-\rho^2}d(Z^{\perp})^{\mathbb{Q}} \\
&= dW^{\mathbb{P}} + (\rho\frac{\mu_u}{\sqrt{v_u}} + \sqrt{1-\rho^2}\gamma_u)du.
\end{aligned} \tag{4.5}$$

The change of measure from $\mathbb{P}$ to $\mathbb{Q}$ can therefore be noted as

$$dW_s^{\mathbb{P}} = dW_s^{\mathbb{Q}} + \lambda_s ds \tag{4.6}$$

---

[6]Two measures $\mathbb{P}$ and $\mathbb{Q}$ are equivalent if for any $A \in \mathcal{F}$, $\mathbb{P}(A) = 0$ iff $\mathbb{Q}(A) = 0$. If, in addition, the discounted price process is a martingale under $\mathbb{Q}$ then $\mathbb{Q}$ is an equivalent martingale measure.

Under the physical measure $\mathbb{P}$, the variance process v simulates the realized variance from market data. Using (4.1) and as established in (4.6), the variance process can be expressed via the pricing measure $\mathbb{Q}$ so that, assuming

$$
\begin{aligned}
v_u &= \mathbb{E}^{\mathbb{P}}[v_u|\mathcal{F}_t]\mathcal{E}\left(\eta\tilde{W}_t^{\mathbb{Q}}(u)\right)\exp\left(\eta\sqrt{2H}\int_t^u (u-s)^{H-\frac{1}{2}}\lambda_s ds\right) \\
&= \xi_t(u)\mathcal{E}\left(\eta\tilde{W}_t^{\mathbb{Q}}(u)\right),
\end{aligned}
$$

with the forward variance curve

$$
\begin{aligned}
\xi_t(u) &= \mathbb{E}^{\mathbb{P}}[v_u|\mathcal{F}_t]\exp\left(\eta\sqrt{2H}\int_t^u (u-s)^{H-\frac{1}{2}}\lambda_s ds\right) \\
&= \mathbb{E}^{\mathbb{Q}}[v_u|\mathcal{F}_t].
\end{aligned}
$$

The rBergomi model is non-Markovian in the instantaneous variance v. As a consequence, the pricing model (4.2) is given under the risk-neutral pricing measure $\mathbb{Q}$ by

$$
\begin{aligned}
dS_u &= \sqrt{v_u}S_u dZ_u^{\mathbb{Q}} \\
v_u &= \xi_t(u)\mathcal{E}\left(\eta\tilde{W}_t^{\mathbb{Q}}(u)\right),
\end{aligned} \tag{4.7}
$$

where

$$
\tilde{W}_t^{\mathbb{Q}}(u) := \sqrt{2H}\int_t^u |u-s|^{H-\frac{1}{2}}dW_s^{\mathbb{Q}}.
$$

It can be noted that the instantaneous variance process v, expressed with the forward variance ξ_t, is a non-Markovian generalization of the Bergomi model, in the sense that $\mathbb{E}^{\mathbb{Q}}[v_u|\mathcal{F}_t] \neq \mathbb{E}^{\mathbb{Q}}[v_u|v_t]$.

4.4   Pricing under rough Bergomi

Under the pricing measure $\mathbb{Q}$ at a given time equal to 0, the scheme used to simulate the model reads

$$
\begin{aligned}
S_t &= S_0 \exp\left[\int_0^t \sqrt{v_s}dZ_s^{\mathbb{Q}} - \frac{1}{2}\int_0^t v_s ds\right] \\
v_t &= \xi_0(t)\exp\left[2\nu C_H \int_0^t \frac{dW_u^{\mathbb{Q}}}{(t-u)^{1/2-H}} - \frac{\nu^2 C_H^2}{H}t^{2H}\right] \\
d[Z^{\mathbb{Q}}, W^{\mathbb{Q}}]_t &= \rho dt.
\end{aligned}
$$

Firstly, the simulation of the Volterra process $\left(\int_0^t \frac{dW_u^{\mathbb{Q}}}{(t-u)^{1/2-H}}\right)_{t\geq 0}$ is done using the hybrid scheme or the generalised fractional operators method. Then, after extracting the standard Brownian motion $\left(W_t^{\mathbb{Q}}\right)_{t\geq 0}$ driving the Volterra process, it is correlated with $Z^{\mathbb{Q}}$ by a coefficient ρ. Finally, the stock price process S is simulated using a forward Euler scheme.

Algorithm 4.1. Stock price simulation under rough Bergomi

1. Fix an equidistant grid $\mathcal{G} = \{t_0 = 0, t_1 = \frac{1}{n}, \ldots, t_{\lfloor nT \rfloor} = \frac{\lfloor nT \rfloor}{n}\}$ for $T > 0$

2. Simulate a Volterra process $\mathcal{V}_t = \int_0^t \frac{dW_u^{\mathbb{Q}}}{(t-u)^{1/2-H}}, \; t \in \mathcal{G}$

3. Compute the variance process v using the Volterra process

$$v_t = \xi_0(t)\mathcal{E}\left(2\nu C_H \mathcal{V}_t\right), \; t \in \mathcal{G}$$

4. Extract the path of the standard Brownian motion $W^{\mathbb{Q}}$ which drives the Volterra process, with W^n as defined in (2.5)

$$W_{t_i}^{\mathbb{Q}} = W_{t_{i-1}}^{\mathbb{Q}} + n^{H-1/2}(\mathcal{V}_{t_i} - \mathcal{V}_{t_{i-1}}), \quad \text{for } i = 1, \cdots, \kappa$$
$$W_{t_i}^{\mathbb{Q}} = W_{t_{i-1}}^{\mathbb{Q}} + W_{i-1}^n, \qquad\qquad \text{for } i > \kappa$$

5. Correlate the stock price driven by $Z^{\mathbb{Q}}$ and the variance processes driven by the Volterra process driven by $W^{\mathbb{Q}}$ through

$$Z_{t_i}^{\mathbb{Q}} - Z_{t_{i-1}}^{\mathbb{Q}} = \rho\left(W_{t_i}^{\mathbb{Q}} - W_{t_{i-1}}^{\mathbb{Q}}\right) + \sqrt{1-\rho^2}\left(W_{t_i}^{\mathbb{Q}\perp} - W_{t_{i-1}}^{\mathbb{Q}\perp}\right),$$

where $W^{\mathbb{Q}\perp}$ is a standard Brownian motion independent of $W^{\mathbb{Q}}$

6. Simulate the stock price process S using the forward Euler scheme

$$S_{t_i} = S_{t_{i-1}} + \sqrt{v_{t_{i-1}}}S_{t_{i-1}}\left(Z_{t_i}^{\mathbb{Q}} - Z_{t_{i-1}}^{\mathbb{Q}}\right)$$

Then, to price a security at time t with maturity $T \geq t$ and payoff f, a Monte-Carlo simulation of the discounted payoff helps approximate the risk-neutral valuation formula

$$\mathbb{E}^{\mathbb{Q}}\left[e^{-\int_t^T r_s ds}f(S)|\mathcal{F}_t\right],$$

where r is the risk-free interest rate.

For example, to price a European Call option with maturity T and strike K at time 0, assuming that $r = 0$, one may price

$$C_0 = \mathbb{E}^{\mathbb{Q}}\left[(S_T - K)_+\right].$$

In practice, we use the Python implementation of the rough Bergomi model by McCrickerd [20].

4.5   Calibration

Calibrating the rBergomi model to at-the-money volatility smiles allows to find the parameters required to simulate price paths in our model: H, ρ and also η which gives ν through $\eta = \frac{2\nu C_H}{\sqrt{2H}}$. The calibration is done on the SPX index as of 10/03/2017 to market data collected from Bloomberg/Janus Henderson Investors and the results are consolidated in 2. In addition to the three parameters, the model also takes as a calibration parameter the initial forward variance curve ξ_0 as constant.

4.5.1   Objective function

The objective function is going to be minimized for calibration purposes. The parameters mentioned above are indeed calibrated so as to minimize the 2-norm of the vector of points. This vector represents the difference between the vector of market data implied volatilities σ_{mkt} and the vector of implied volatilities $\hat{\sigma}_{rB}$ drawn from the rBergomi model: both vectors contain implied volatilities for the same range of log-moneyness. To recap, the least squares method yielding the model parameters is written

$$\underset{\mathcal{P}}{\mathrm{argmin}}\, g(k,\tau) := \underset{\mathcal{P}}{\mathrm{argmin}}\, \|\hat{\sigma}_{rB}(k,\tau) - \sigma_{mkt}(k,\tau)\|^2 \,,$$

where $\mathcal{P} = \{H, \rho, \eta, \xi\}$ stands for the set of parameters, τ denotes time to maturity and $k = \log\dfrac{K}{F}$ is the log-moneyness.

4.5.2   Numerical results

To minimize the objective function, a sequential least squares programming algorithm [18] is used. It is worth noticing that time of execution increases with time to maturity. Moreover, the time-independence assumption can be questioned. Indeed, the three parameters H, ρ and η, sufficient to describe the rBergomi model, present some variations over time, especially for small maturities: the Hurst exponent H is of order 0.05 for a one-week maturity whereas it is of order 0.1 for maturities greater than one-month.

We will also note that the values of the forward-variance curve parameter, taken as inputs in our calibration model, are really close to the volatility swap strike prices ξ^{MKT} of the SPX index observed in the market.

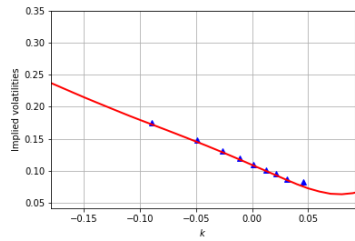| T	H	ρ	η	ξ	ξ^{MKT}
0.020	0.055	-0.886	1.799	0.009	
0.083	0.120	-0.917	1.833	0.010	0.013
0.171	0.125	-0.919	1.820	0.015	0.018
0.262	0.155	-0.918	1.845	0.018	0.020
0.520	0.122	-0.916	1.812	0.024	0.026
0.778	0.126	-0.913	1.811	0.030	0.029
1.036	0.114	-0.912	1.805	0.031	0.031
1.552	0.104	-0.870	1.822	0.036	0.034
2.067	0.115	-0.831	1.827	0.042	0.039

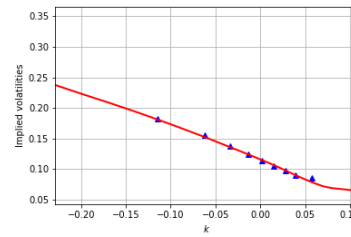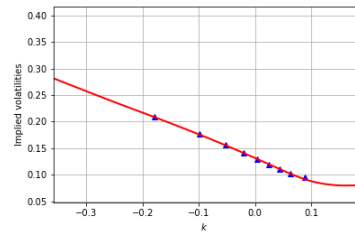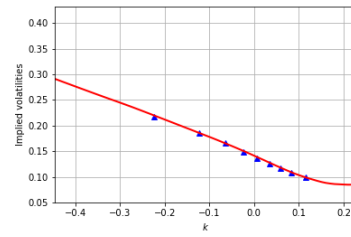Table 2: Results of the rBergomi calibration on volatility smiles
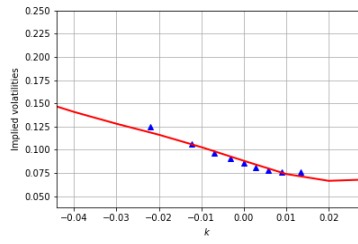
(a) $T = 0.020$
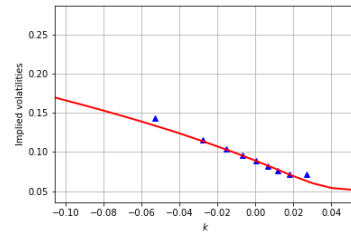
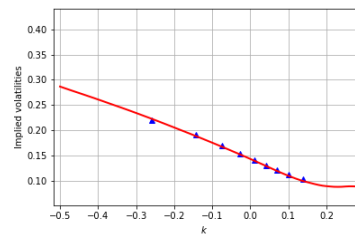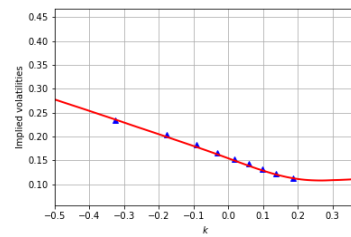(b) $T = 0.083$

(c) $T = 0.171$

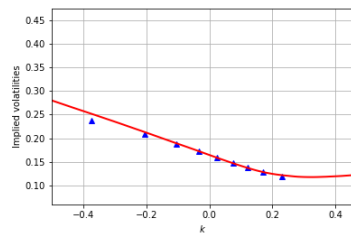(d) $T = 0.262$

(e) $T = 0.520$

(f) $T = 0.778$

(g) $T = 1.036$

(h) $T = 1.552$

(i) $T = 2.067$

Figure 7: Calibration of rBergomi to volatility smiles. Source: Bloomberg/Janus Henderson Investors

4.6   Volatility skew

4.6.1   Definition and mapping

The at-the-money volatility skew is given by

$$\psi(\tau) := \left| \frac{\partial}{\partial k} \tilde{\sigma}(k, \tau) \right|_{k=0},$$

where k denotes the log-moneyness, τ the time to maturity and $\tilde{\sigma}$ the implied volatility in terms of k. The term structure of the market data at-the-money-forward volatility skew is defined as

$$\Psi(\tau) = \left| \frac{\partial}{\partial K} \sigma_{mkt}(K, \tau) \right|_{K=F},$$

where K is the strike, F the forward price and σ_{mkt} the market implied volatility. Taking $k = \log \frac{K}{F}$, we set $\tilde{\sigma}(k, \tau) = \sigma_{mkt}(K, \tau)$ so that

$$\frac{\partial}{\partial K} \sigma_{mkt}(K, \tau) = \frac{\partial}{\partial k} \tilde{\sigma}(k, \tau) \cdot \frac{\partial k}{\partial K} = \frac{1}{K} \frac{\partial}{\partial k} \tilde{\sigma}(k, \tau).$$

Therefore the data, expressed in terms of strike K, is mapped to data expressed in log-moneyness k and the at-the-money-forward volatility skew is

$$\psi(\tau) = F \left| \frac{\partial}{\partial K} \sigma_{mkt}(K, T) \right|_{K=F}.$$

4.6.2   Numerical results

To estimate the at-the-money volatility skew, a central finite difference method is applied to implied volatilities drawn from the rBergomi model in the neighbourhood of $k = 0$. Letting $h > 0$, then for each τ in $\mathcal{T}$, the simulation interval, the approximation of ψ is given by

$$\psi(\tau) \simeq \left| \frac{\hat{\sigma}_{rB}(h, \tau) - \hat{\sigma}_{rB}(-h, \tau)}{2h} \right|.$$

In practice, taking $h = 1e - 3$ allows a good approximation of the derivative in the neighborhood of zero.

In addition, market data skew is actually obtained by calibrating the SVI *stochastic volatility inspired* model to market data implied volatility. The SVI model [10] [11] is calibrated to the volatility surface using a set of parameters $\lambda = \{a, b, \rho, m, \sigma\}$ such that the total implied variance is expressed, for $k \in \mathbb{R}$, by

$$\sigma_{imp}^2(k; \lambda) = a + b \left\{ \rho(k - m) + \sqrt{(k - m)^2 + \sigma^2} \right\},$$

where $a \in \mathbb{R}$, $b \geq 0$, $|\rho| < 1$, $m \in \mathbb{R}$ and $\sigma > 0$. In addition, $\sigma_{imp}^2(k; \lambda)$ stays positive and is ensured by the condition $a + b\sigma\sqrt{1 - \rho^2} \geq 0$.

Therefore, by construction, as the smile generated from rBergomi fits the market data, the skew generated/approximated by rBergomi should fit the skew obtained by the SVI model.
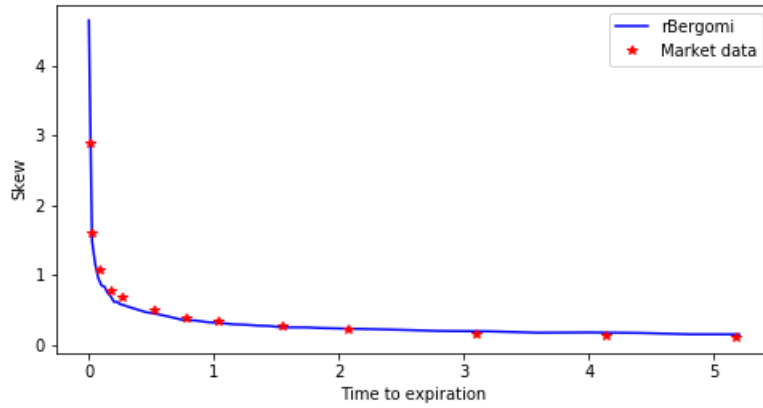

Figure 8: SPX at-the-money-forward volatility skew

4.6.3   Approximation of skew

The term structure of at-the-money volatility skew can be approximated by a power-law function of time to expiry, as shown by Gatheral, Jaisson and Rosenbaum [12]. In this context, the function $\tau \mapsto A\tau^{-\alpha}$ is fitted to the few points of the skew term structure.
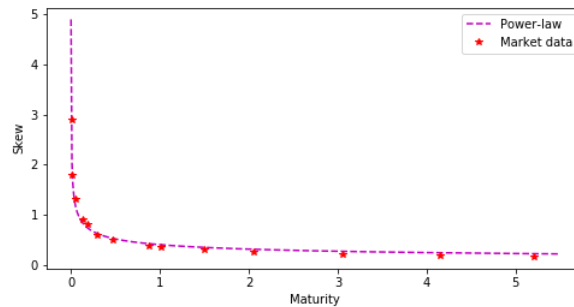
Figure 9: Power-law fit to the term structure of SPX at-the-money-forward volatility skew

As a result, the parameters obtained via this fit are $A = 0.40$ and $\alpha = 0.36$. This function has motivated the use of a power-law kernel function to model volatility, leading to the rBergomi model. Indeed, when volatility is driven by a fBM with Hurst parameter H, then the skew is proportional to $\tau^{H-1/2}$. As α is of order 0.4, H should be of order 0.1, which has been discussed previously.

Similarly, other functions could be fit to the term structure of at-the-money volatility skew. As an

instance, we choose the function

$$\tau \mapsto A\tau^{-\alpha}\mathrm{e}^{-\beta\tau},$$

where $\beta > 0$. In this setting, the parameters of the function are $A = 0.45$, $\alpha = 0.34$ and $\beta = 0.15$.
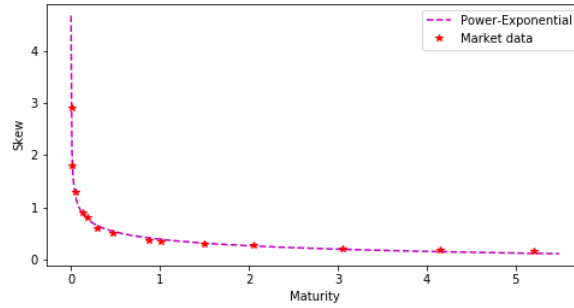

Figure 10: Alternative fit to the term structure of SPX at-the-money-forward volatility skew

4.6.4 Change of kernel

As the power-law fit motivated the use of a power-law kernel in our volatility model (4.7), this new fit can inspire us to choose a kernel such that

$$K(t, s) = (t - s)^{H-1/2}\mathrm{e}^{-\beta(t-s)}.$$

The new process to simulate would thus be, for $t > 0$

$$D_t := \int_0^t (t - s)^{H-1/2}\mathrm{e}^{-\beta(t-s)}dW_s.$$

D_t is Gaussian with the following properties

$$\mathbb{E}[D_t] = 0$$

$$\mathbb{E}[D_t^2] = \int_0^t (t - s)^{2H-1}\mathrm{e}^{-2\beta(t-s)}ds$$

$$= \int_0^t s^{2H-1}\mathrm{e}^{-2\beta s}ds$$

$$= \frac{1}{(2\beta)^{2H}} \int_0^{2\beta t} s^{2H-1}\mathrm{e}^{-s}ds$$

We recognize the lower incomplete gamma function given by

$$\gamma(a, x) = \int_0^x s^{a-1}\mathrm{e}^{-s}ds$$

$$= a^{-1}x^a\mathrm{e}^{-x}{}_1F_1(1, 1 + a, x)$$

$$= a^{-1}x^a{}_1F_1(a, 1 + a, -x),$$

where $_1F_1$ is the confluent hypergeometric function of the first kind, defined, for $a, b \in \mathbb{R}$ and $z \geq 0$, as

$$_1F_1(a, b, z) = \sum_{k=0}^{\infty} \frac{(a)_k}{(b)_k} \frac{z^k}{k!},$$

where $(.)_k$ is the rising factorial.

In fact, D_t can be simulated by a left-point approximation as previously seen 2.24. Discretizing $[0, t]$ such that $0 = t_0 < \cdots < t_n = t$ with $t_i = \frac{i}{n}$ for every $i \in \{0, \cdots, n\}$, as

$$D_t = \sum_{i=0}^{n-1} \int_{t_i}^{t_{i+1}} (t-s)^{H-1/2} e^{-\beta(t-s)} dW_s$$

the approximaiton reads

$$\begin{aligned} \widetilde{D_t} &= \sum_{i=0}^{n-1} (t-t_i)^{H-1/2} e^{-\beta(t-t_i)} (W_{t_{i+1}} - W_{t_i}) \\ &= \sum_{i=0}^{n-1} (t_i)^{H-1/2} e^{-\beta t_i} (W_{t-t_i} - W_{t-t_{i+1}}) \\ &= (1/n)^H \sum_{i=0}^{n-1} i^{H-1/2} e^{-\beta i/n} Z_{n-i}, \end{aligned}$$

where $(Z_i)_{i \in \{1, \cdots, n\}}$ are n independently drawn standard Gaussian random variables.

4.7 Forward-start options

4.7.1 Definition

The sensitivity to forward-smile risk, described as the risk coming from the market future implied volatility and its uncertainty, is found in many options. These options, such as the Forward-start options, or cliquets, are priced given the distribution of forward returns in the model, as described by Bergomi [5]. The payoff of a Forward-start option involves the prices of the security at two different dates T_1 and T_2 such that $T_1 < T_2$. This payoff can be seen as a function of the forward return $\frac{S_{T_2}}{S_{T_1}} - k$ with $k > 0$ defining the moneyness of the contract, or, in a simpler way, is expressed as

$$(S_{T_2} - k S_{T_1})_+ .$$

Pricing a payoff involving such a ratio requires modeling assumptions and further allows to generate implied volatility surfaces. Indeed, to obtain the forward smile $\hat{\sigma}_k^{T_1, T_2}$, Forward-start Call options are priced for different values of moneyness k and the implied Black-Scholes volatility stands for $\hat{\sigma}_k^{T_1, T_2}$. The forward smile represents the expected future implied volatility for moneyness k: all possible realizations of future smiles are averaged to give $\hat{\sigma}_k^{T_1, T_2}$.

The instantaneous volatility σ is time-dependent, due to the nature of the Forward-start option, whose price depends on S_{T_1} and S_{T_2}. The Black-Scholes implied volatility for maturity T is given by

$$\hat{\sigma}_T^2 := \int_t^T \sigma(u)^2 du.$$

The price of a Forward-start option is independent of the stock price S but depends on the forward volatility $\hat{\sigma}_{T_1,T_2}$ or the integrated variance over $[T_1, T_2]$ such that

$$\hat{\sigma}_{T_1,T_2}^2 := \int_{T_1}^{T_2} \sigma(u)^2 du$$
$$= \frac{(T_2 - t)\hat{\sigma}_{T_2}^2 - (T_1 - t)\hat{\sigma}_{T_1}^2}{T_2 - T_1}.$$

4.7.2   Implied volatilities

To price Forward-start options under the rough Bergomi model, a Monte-Carlo method is used to approximate the price. The generation of a price path is executed as before and we extract the values on a path at T_1 amd T_2.
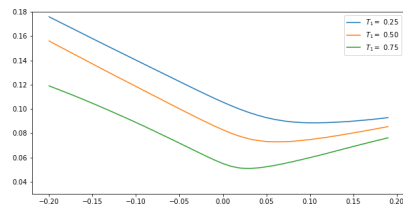
Algorithm 4.2. Implied volatilities of Forward-start options under rBergomi

1. Set a range $\{0.75, \cdots, 2.75\}$ of step 0.25 for maturities T_2

2. Set a range $\{0.25, \cdots, T_2 - 0.25\}$ of step 0.25 for starting dates T_1

3. Simulate price paths in $[0, T_2]$ under rBergomi using 4.1

4. For each $\alpha \in [-0.2, 0.2]$, indicating log-moneyness, compute $(S_{T_2} - S_{T_1}(1 + \alpha))_+$, the payoffs, and use the Monte-Carlo method to compute the price of the Forward-start options

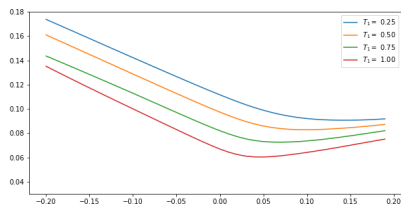5. Retrieve implied volatilities from Black-Scholes option pricing formula using root-finding functions.

As maturity increases, the spread between implied volatility of starting dates (T_1) close to 0 and starting dates close to maturity seem to decrease.
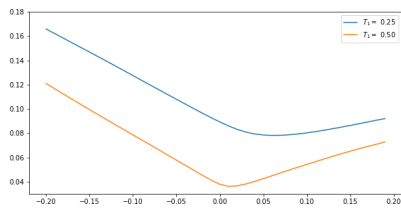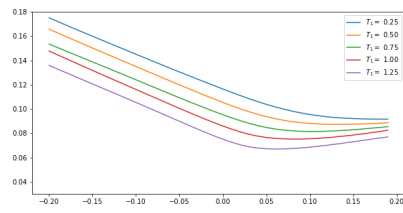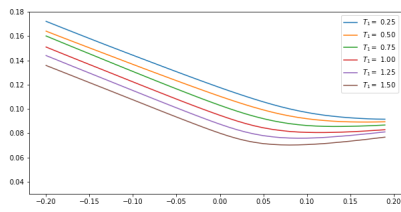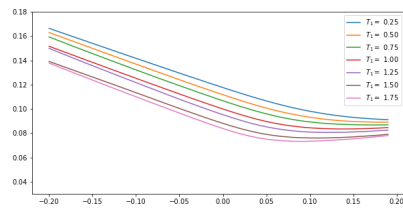
(a) $T_2 = 0.75$

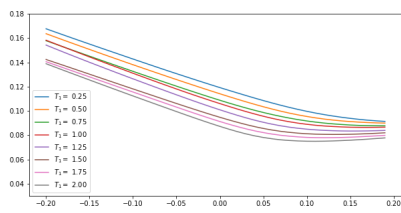(b) $T_2 = 1.00$

(c) $T_2 = 1.25$
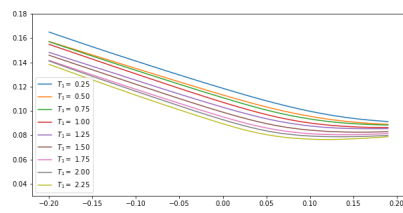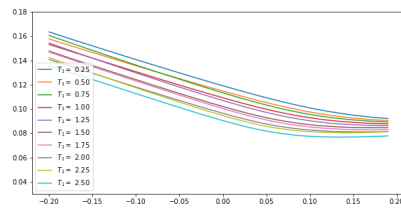
(d) $T_2 = 1.50$

(e) $T_2 = 1.75$

(f) $T_2 = 2.00$

(g) $T_2 = 2.25$

(h) $T_2 = 2.50$

(i) $T_2 = 2.75$

Figure 11: Implied volatilities of Forward-start options under rBergomi

5   VIX

VIX dynamics under the rBergomi model are mentioned by Bayer, Friz and Gatheral [2] and they introduce a log-normal approximation, restudied by Jacquier, Martini and Muguruza [17] to compare the first and second moments of the VIX distribution.

5.1   VIX index

The VIX index is a measure of 30-day expected volatility of the U.S. stock market published by the Chicago Board Options Exchange (CBOE). Derived from real-time mid-quote prices of S&P 500 Index Call and Put options, the VIX index is widely used as a volatility indicator. The generalized formula used in the VIX Index calculation is

$$VIX^2 = \frac{2}{T} \sum_i \frac{\Delta K_i}{K_i^2} Q_i(K_i) - \frac{1}{T} \left(\frac{F}{K_0} - 1 \right)^2,$$

where K_i is the strike price of the ith OTM option, ΔK_i is the interval between strike prices K_{i+1} and K_{i-1}, $Q_i(K_i)$ is the undiscounted mid price for the option with strike K_i and K_0 the greatest strike price below the forward index level F. The VIX index thus provides an instantaneous view of how much the S&P 500 Index is expected to fluctuate within the next 30 days.

The volatility index VIX can also be seen as an approximation of the value of a one-month variance swap on S&P 500. As a reminder, the payoff of a variance swap contract at time 0 with maturity T is

$$RV^{0,T} - K,$$

where

$$RV^{0,T} := \frac{d}{M} \sum_{i=1}^{M} \log \left(\frac{S_{t_i}}{S_{t_{i-1}}} \right)^2,$$

K is the strike, d the factor that annualized realized variance (usually 252), and $(S_{t_i})_{i \in \{0,...,M\}}$ a time series of stock prices. For stock prices modelled by geometric Brownian motion or log-normal dynamics

$$dS_t = r_t S_t dt + \sigma_t S_t dW_t, \tag{5.1}$$

the squared-process of log-returns on an interval of the partitioned time is approximately

$$\log \left(\frac{S_{t_i}}{S_{t_{i-1}}} \right)^2 \approx \sigma_{t_{i-1}}^2 \left(t_i - t_{i-1} \right),$$

hence, in a continuous-time setting,

$$RV^{0,T} \approx \frac{1}{T} \int_0^T \sigma_t^2 dt$$

Applying Itô's lemma to process (5.1) describing stock prices, one has

$$d \log S_t = \frac{dS_t}{S_t} - \frac{1}{2}\frac{1}{S_t^2}d[S]_t = \frac{dS_t}{S_t} - \frac{1}{2}\sigma_t^2 dt.$$

As a result, the integrated variance process is expressed as

$$\frac{1}{T}\int_0^T \sigma_t^2 dt = \frac{2}{T}\int_0^T \frac{dS_t}{S_t} - \frac{2}{T}\log\left(\frac{S_T}{S_0}\right).$$

The price of a variance swap, as the expected value of the integrated variance under the risk neutral measure, is statically replicated by a portfolio of OTM vanilla options with a range of strikes and a maturity T:

$$\mathbb{E}^{\mathbb{Q}}\left[\frac{1}{T}\int_0^T \sigma_t^2 dt\right] = \frac{2}{T}\left(\int_{-\infty}^0 \text{Put}(k,T)dk + \int_0^\infty \text{Call}(k,T)dk\right),$$

where $\text{Put}(k,T)$ and $\text{Call}(k,T)$ are respectively Put and Call option prices with maturity T as a function of log-moneyness $k = \log\frac{K}{F}$, where K is the strike of the option and F the forward price of the underlying. Similarly, considering the strike K only, the expression of the price of a variance swap [7] is

$$\mathbb{E}^{\mathbb{Q}}\left[\frac{1}{T}\int_0^T \sigma_t^2 dt\right] = \frac{2}{T}\left(\int_0^F \frac{\text{Put}(K,T)}{K^2}dK + \int_F^\infty \frac{\text{Call}(K,T)}{K^2}dK\right).$$

To conclude on the relation between the VIX index and variance swap contracts on S&P 500 with maturity one-month, using the fair strike of a variance swap gives

$$VIX^2 = \mathbb{E}^{\mathbb{Q}}\left[\frac{1}{T}\int_0^T \sigma_t^2 dt\right],$$
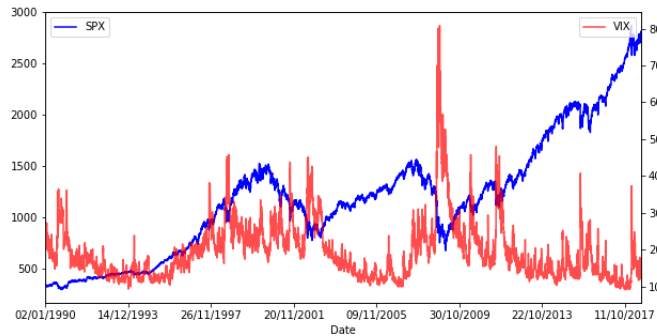
where $T = 30$ days.

Figure 12: S&P 500 and VIX levels

5.2   VIX dynamics

The dynamics of VIX are analyzed by Jacquier, Martini and Muguruza [17] and given under the rough Bergomi model by

$$VIX_T = \left(\frac{1}{\Delta} \int_T^{T+\Delta} \xi_0(t)\eta_T(t) \exp\left[\frac{\nu^2 C_H^2}{H} \left((t-T)^{2H} - t^{2H} \right) \right] dt \right)^{\frac{1}{2}},$$

where, for any $t \geq T$ and $Z^{\mathbb{Q}}$ a standard Brownian motion,

$$\eta_T(t) := \exp\left(2\nu C_H \int_0^T \frac{1}{(t-u)^{1/2-H}} dZ_u^{\mathbb{Q}} \right).$$

The proof can be found in A.

As a consequence, the forward variance curve $\xi_t(\cdot)$ in the rBergomi model has log-normal dynamics and is represented, for any $t \geq T$, by

$$\xi_T(t) = \xi_0(t)\eta_T(t) \exp\left[\frac{\nu^2 C_H^2}{H} \left((t-T)^{2H} - t^{2H} \right) \right].$$

VIX Futures are standard Futures contracts on the VIX volatility index, the measure of 30-day expected volatility of the S&P 500 Index. As standard Futures contracts in general, the risk-neutral price for a VIX Futures contract with maturity $T > 0$ is

$$FV_{IX_T} := \mathbb{E}^{\mathbb{Q}}\left[VIX_T | \mathcal{F}_0 \right], \tag{5.2}$$

where

$$VIX_T = \sqrt{\mathbb{E}^{\mathbb{Q}}\left[\frac{1}{\Delta} \int_T^{T+\Delta} \sigma_t^2 dt \Big| \mathcal{F}_T \right]} = \sqrt{\frac{1}{\Delta} \int_T^{T+\Delta} \mathbb{E}^{\mathbb{Q}}\left[\sigma_t^2 | \mathcal{F}_T \right] dt} = \sqrt{\frac{1}{\Delta} \int_T^{T+\Delta} \xi_T(t) dt}, \tag{5.3}$$

where $\Delta = 30$ days.

Moreover, options on the CBOE Volatility Index VIX have been traded for several years now, and VIX Call options are defined here by

$$CV_{IX_T} := \mathbb{E}^{\mathbb{Q}}\left[e^{-\int_0^T r_s ds} \left(VIX_T - K \right)_+ | \mathcal{F}_0 \right]. \tag{5.4}$$

5.3   Numerical simulations

Pricing VIX derivatives with different maturities under the rough Bergomi model requires simulation methods. In particular, VIX processes are driven by the Gaussian process, for $t \in [T, T+\Delta]$,

$$V_t^T = \int_0^T \frac{1}{(t-u)^{1/2-H}} dZ_u^{\mathbb{Q}}.$$

Properties 5.1. The process V^T has the following properties, for any $t, s \in [T, T+\Delta]$ and $t < s$:

1. $\mathbb{E}[V_t^T] = 0$,

2. $\mathbb{V}[V_t^T] = \dfrac{t^{2H} - (t-T)^{2H}}{2H}$

3. $\mathbb{E}[V_t^T V_s^T] = \displaystyle\int_0^T (t-u)^{H-1/2}(s-u)^{H-1/2}du$

$$= \frac{(s-t)^{H_-}}{H_+}\left[-(t-T)^{H_+}F\left(\frac{T-t}{s-t}\right) + t^{H_+}F\left(\frac{-t}{s-t}\right)\right],$$

where $H\pm = H \pm \dfrac{1}{2}$ and $F(\cdot) = {}_2F_1(-H_-, H_+, H_+ + 1, \cdot)$ with ${}_2F_1$ the Gaussian hypergeometric function.

5.3.1 Forward Euler approach

The forward Euler scheme is used to simulate the process V_τ^T, for $\tau \in [T, T+\Delta]$. On the equidistant grid $0 = t_0 < t_1 = \frac{1}{n} < \cdots < t_{\lfloor nT \rfloor} = \frac{\lfloor nT \rfloor}{n}$, the integral is approximated by a discrete sum such that, for $\tau \in [T, T + \Delta]$,

$$V_\tau^T \simeq \sum_{i=1}^{n_T} \frac{1}{(\tau - t_{i-1})^{1/2-H}}\left(Z_{t_i}^\mathbb{Q} - Z_{t_{i-1}}^\mathbb{Q}\right),$$

where $n_T = \lfloor nT \rfloor$ and $Z^\mathbb{Q}$ is a standard Brownian motion. Now, the integral part involved in the VIX_T computation is estimated via numerical integration.

Algorithm 5.2. VIX simulation with the forward Euler approach

1. Fix an equidistant grid $\{0 = t_0, t_1 = \frac{1}{n}, \ldots, t_{\lfloor nT \rfloor} = \frac{\lfloor nT \rfloor}{n}\}$ for $T > 0$

2. Simulate $(Z_i)_{i \in \{0, \ldots, n_T-1\}}$ independent standard normal variables so that

$$Z_{t_i}^\mathbb{Q} - Z_{t_{i-1}}^\mathbb{Q} = \sqrt{\frac{1}{n}} Z_{i-1}$$

3. Fix an equidistant grid $\{\tau_0, \ldots, \tau_N\}$ on $[T, T + \Delta]$ and approximate the continuous-time process V^T by discretizing it with $\tilde{V}^T$ using the forward Euler approach:

$$\tilde{V}_{\tau_j}^T \simeq \sum_{i=1}^{n_T} \frac{1}{(\tau_j - t_{i-1})^{1/2-H}}\left(Z_{t_i}^\mathbb{Q} - Z_{t_{i-1}}^\mathbb{Q}\right), \text{ for } j \in \{0, \ldots, N\}$$

4. Simulate the forward variance curve in the rBergomi model on the same grid as $\widetilde{V}_T$:

$$\tilde{\xi}_T(\tau_j) = \xi_0(\tau_j)\exp\left(2\nu C_H \tilde{V}_{\tau_j}^T\right)\exp\left(\frac{\nu^2 C_H^2}{H}\left[(\tau_j - T)^{2H} - \tau_j^{2H}\right]\right), \text{ for } j \in \{0, \ldots, N\}$$

5. Compute VIX_T^2 using numerical integration methods, such as the trapezoidal rule

$$VIX_T^2 = \frac{1}{\Delta}\sum_{j=0}^{N-1}\frac{\tilde{\xi}_T(\tau_j) + \tilde{\xi}_T(\tau_{j-1})}{2}(\tau_j - \tau_{j-1})$$

$$= \frac{1}{2N}\sum_{j=0}^{N-1}\tilde{\xi}_T(\tau_j) + \tilde{\xi}_T(\tau_{j-1}).$$

The simulation of the forward Euler approach is there realized in two main step: the generation of standard normal variables, with complexity $\mathcal{O}(n)$ and the construction of the process $(V_\tau^T)_{\tau \in [T, T+\Delta]}$, with complexity $\mathcal{O}(n)$.

5.3.2 Truncated Cholesky

Another method to simulate V_τ^T, for $\tau \in [T, T+\Delta]$, is the truncated Cholesky method. It is based on the Cholesky decomposition of the covariance matrix whose structure is known and given in 5.1. It is important to note that the computational complexity of the Cholesky decomposition makes this method really slow. In addition, there is no guarantee that the Cholesky method can even be applied for the covariance matrix of V^T as the positive-definite property is not verified numerically.

Algorithm 5.3. VIX simulation with the truncated Cholesky approach

1. Fix an equidistant grid $\{\tau_1, \dots, \tau_N\}$ on $[T, T+\Delta]$

2. For $\tau \in \{\tau_1, \dots, \tau_8\}$, compute the variance matrix of V_τ^T: for $i < j \in \{1, \cdots, 8\}$

$$\mathbb{E}[V_{\tau_i}^T V_{\tau_j}^T] = \frac{(\tau_j - \tau_i)^{H_-}}{H_+} \left[-(\tau_i - T)^{H_+} F\left(\frac{T - \tau_i}{\tau_j - \tau_i} \right) + \tau_i^{H_+} F\left(\frac{-\tau_i}{\tau_j - \tau_i} \right) \right]$$

3. For $\tau \in \{\tau_9, \dots, \tau_N\}$ by correlating $V_{\tau_j}^T$ and $V_{\tau_{j-1}}^T$ and rescaling, for $j \in \{9, \cdots, N\}$,

$$V_{\tau_j}^T = \sqrt{\mathbb{V}(V_{\tau_j}^T)} \left(\rho_j \frac{V_{\tau_{j-1}}^T}{\sqrt{\mathbb{V}(V_{\tau_{j-1}}^T)}} + \sqrt{1 - \rho_j^2} Z_j \right),$$

where $\rho_j = \frac{\mathbb{E}[V_{\tau_j}^T V_{\tau_{j-1}}^T]}{\sqrt{\mathbb{V}(V_{\tau_j}^T) \mathbb{V}(V_{\tau_{j-1}}^T)}} = \text{corr}\left(V_{\tau_j}^T, V_{\tau_{j-1}}^T \right)$ and $Z = (Z_j)_{j \in \{9, \cdots, N\}}$ are independently drawn standard normal variables.

4. Simulate the forward variance curve in the rBergomi model on the same grid as $\widetilde{V}_T$, as seen in the previous algorithm 5.2

5. Compute VIX_T^2 using numerical integration methods

5.4 Log-normal approximations

5.4.1 Jacquier-Martini-Muguruza approach

Considering the expression (5.3) for the VIX volatility index, let us define the $\mathcal{F}_T$-measurable random variable

$$X_T = \int_T^{T+\Delta} \xi_T(t) dt.$$

As ξ_T is log-normal, and using the approximation of integrals by Riemann sums, the approximation made in this part consists in the log-normality of X_T. However, the sum of log-normal random variables is not said to be log-normal. Relying on Dufresne's proof [9] that the integral of log-normal

variables converges asymptotically to a log-normal random variable, under certain conditions, it can be noted that

$$\log X_T \sim N(\mu, \sigma^2).$$

The first two moments of X_T in this configuration read

$$\mathbb{E}^{\mathbb{Q}}[X_T] = \exp\left(\mu + \frac{\sigma^2}{2}\right), \quad \mathbb{E}^{\mathbb{Q}}[X_T^2] = \exp\left(2\mu + 2\sigma^2\right),$$

therefore $\log X_T$ is fully determined by

$$\mu = 2\log \mathbb{E}^{\mathbb{Q}}[X_T] - \frac{1}{2}\log \mathbb{E}^{\mathbb{Q}}[X_T^2],$$

$$\sigma^2 = \log \mathbb{E}^{\mathbb{Q}}[X_T^2] - 2\log \mathbb{E}^{\mathbb{Q}}[X_T].$$

Once again, Jacquier, Martini and Muguruza [17] demonstate the following results regarding the first two moments of X_T:

$$\mathbb{E}^{\mathbb{Q}}[X_T] = \int_{[T,T+\Delta]} \xi_0(t)dt$$

$$\mathbb{E}^{\mathbb{Q}}[X_T^2] = \int_{[T,T+\Delta]^2} \xi_0(u)\xi_0(t) \exp\left[\frac{\nu^2 C_H^2}{H}\left((u-T)^{2H} + (t-T)^{2H} - u^{2H} - t^{2H}\right)\right] \exp\left[\theta_{u,t}\right] dudt,$$

where

$$\theta_{u,t} := \begin{cases} \sigma^2_{\max(u,t),\,\min(u,t)} & \text{if } u \neq t \\ 0 & \text{if } u = t, \end{cases}$$

and

$$\sigma^2_{u,t} := 2\nu^2 C_H^2 \left[\frac{u^{2H} - (u-T)^{2H} + t^{2H} - (t-T)^{2H}}{2H} \right.$$

$$\left. + 2\frac{(u-t)^{H_-}}{H_+}\left[t^{H_+}F\left(\frac{-t}{u-t}\right) - (t-T)^{H_+}F\left(\frac{T-t}{u-t}\right)\right]\right].$$

As a result, the price of a VIX Futures contract is approximated in the log-normal model by

$$FV_{IX_T} \simeq \mathbb{E}^{\mathbb{Q}}\left[\sqrt{\frac{1}{\Delta}X_T}\right] = \sqrt{\frac{1}{\Delta}}\exp\left(\frac{\mu}{2} + \frac{\sigma^2}{8}\right). \tag{5.5}$$

A closed-form formula is also given for VIX Call options (5.4), assuming interest rates are zero:

$$CV_{IX_T} = \sqrt{\frac{1}{\Delta}}\exp\left(\frac{\mu}{2} + \frac{\sigma^2}{8}\right)\mathcal{N}(d_1) - K\mathcal{N}(d_2), \tag{5.6}$$

where

$$d_1 = \frac{1}{\sigma}\left(\mu + \frac{\sigma^2}{2} - \log(K^2\Delta)\right)$$

$$d_2 = d_1 - \frac{\sigma}{2}$$

and $\mathcal{N}$ denotes the cumulative distribution function of the Gaussian random variable.

5.4.2   Bayer, Friz and Gatheral approximation

Bayer, Friz and Gatheral consider X_T as log-normal so that $\log X_T$ has mean $\tilde{\mu}$ and variance $\tilde{\sigma}^2$. In fact, they aim to approximate the variance of $\log X_T$ using

$$\tilde{X}_T = \exp\left(\frac{1}{\Delta}\int_T^{T+\Delta}\mathbb{E}^{\mathbb{Q}}\left[\log v_t|\mathcal{F}_T\right]dt\right). \tag{5.7}$$

The second moment is obtained via this very approximation of X_T, therefore giving the variance

$$\mathbb{V}\left[\log\tilde{X}_T|\mathcal{F}_s\right] = \frac{4\nu^2 C_H^2}{\Delta^2 H_+^2}\int_s^T\left[(T-u+\Delta)^{H_+}-(T-u)^{H_+}\right]^2 du.$$

The first moment of X_T is obtained using Fubini's theorem and the tower property. Indeed, as

$$\mathbb{E}^{\mathbb{Q}}\left[X_T|\mathcal{F}_s\right] = \int_T^{T+\Delta}\xi_s(t)dt,\ \ s\leq T,$$

taking $s=0$ gives

$$\mathbb{E}^{\mathbb{Q}}\left[X_T\right] = \int_T^{T+\Delta}\xi_0(t)dt.$$

The log-normality of X_T gives

$$\mathbb{E}^{\mathbb{Q}}[X_T] = \exp\left(\tilde{\mu}+\frac{\tilde{\sigma}^2}{2}\right),$$

where

$$\tilde{\sigma}^2 = \mathbb{V}\left[\log\tilde{X}_T\right]$$

$$\tilde{\mu} = \log\mathbb{E}^{\mathbb{Q}}[X_T]-\frac{\tilde{\sigma}^2}{2}$$

Similarly to (5.5) and (5.6) and using these expressions for $\tilde{\mu}$ and $\tilde{\sigma}$, the prices of VIX Futures and VIX Call options are obtained in the Bayer-Friz-Gatheral approach.

5.5   Numerical results

One important feature in these methods is the initial forward variance curve ξ_0. The choice of this parameter plays a part in the determination of the instruments' prices. Hence, three scenarios are considered, as in [17]:

1. $\xi_0(t)=\xi_0$

2. $\xi_0(t)=\xi_0(1+t)^2$

3. $\xi_0(t)=\xi_0\sqrt{1+t}$

As regards the other parameters, they are taken similarly as before, i.e.

$$H=0.07,\quad \nu=\frac{\eta\sqrt{2H}}{2C_H}\ \text{with}\ \eta=1.9,\quad \xi_0=0.234^2.$$

As the hybrid scheme is used to simulate the Volterra process, we also need to choose κ. For algorithmic purposes, $\kappa=1$ is taken.

5.5.1   VIX Futures

The simulation of VIX Futures prices using the Euler method is compared with the log-normal approximation of Jacquier, Martini and Muguruza in [17]. The latter is also compared the Bayer-Friz-Gatheral's approximation. Moreover, relative differences (in percentage) between the methods are also shown so as to interpret the simulations.

Firstly, the Euler method uses 10^5 simulations, with a time-grid step of $1/n$ with $n = 500$ and the Volterra process constructed with $N = 500$. The relative differences are, for each scenario, of order 0.5%, differences likely varying due to Monte Carlo simulation error. For scenario 1, longer maturities tend to give slightly bigger differences and oscillations and scenario 3 is much more oscillating than than two other scenarios.
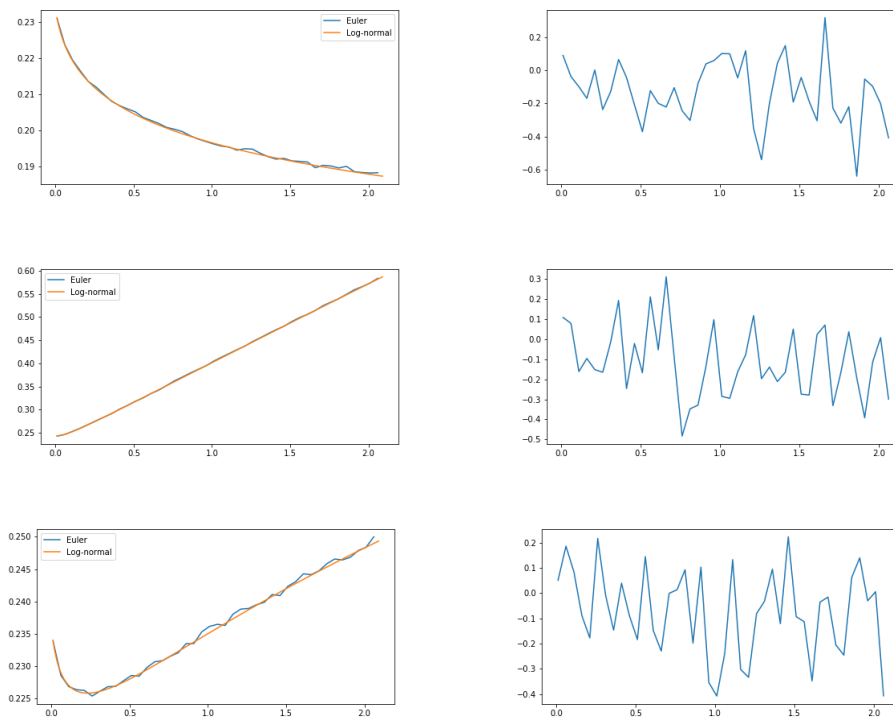

Figure 13: VIX Futures simulations in Euler and Jacquier-Martini-Muguruza approach and the relative differences for scenarios 1, 2 and 3
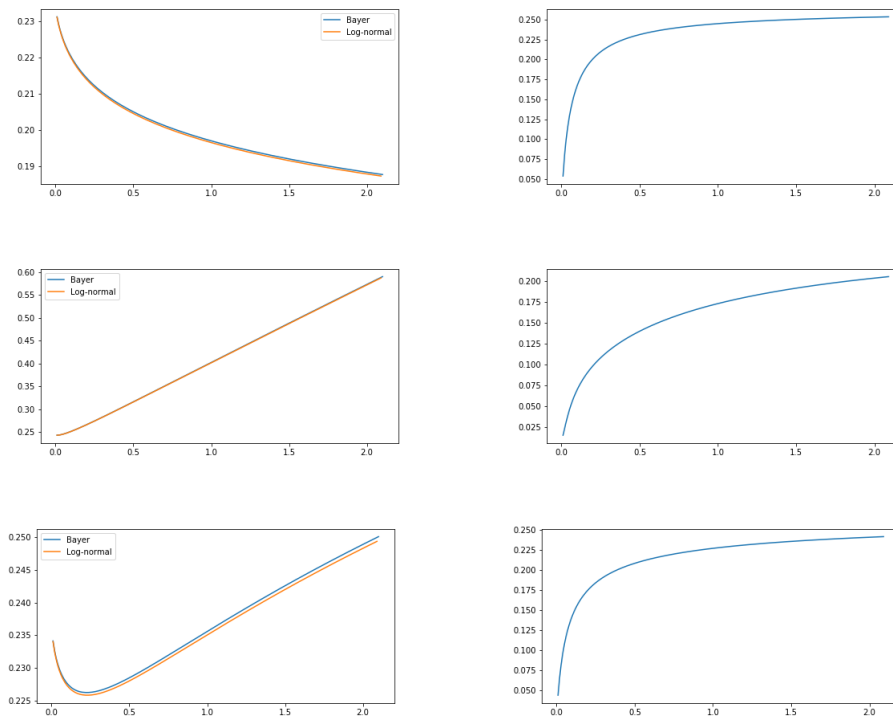
Figure 14: VIX Futures simulations with log-normal approximations and the relative differences for scenarios 1, 2 and 3

5.5.2   VIX options

VIX Call options prices are also computed using the Euler method and the log-normal approximation of Jacquier-Martini-Muguruza using the same settings and parameters as in 5.5.1. The only scenario used here is the constant initial forward curve $\xi_0(t) = \xi_0$ and the simulation is done for three different strikes: at-the-money, in-the-money ($K = 0.01$) and out-of-the-money ($K = 0.1$).
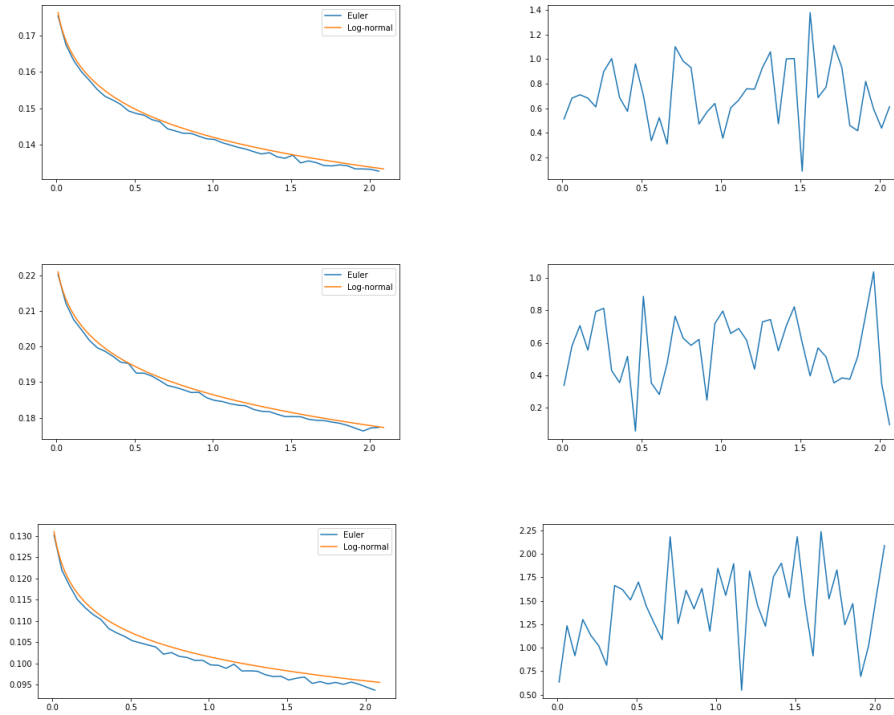

Figure 15: VIX Call options simulations in Euler and log-normal approximations and the relative differences for scenarios 1, 2 and 3

For in-the-money and at-the-money options, the log-normal approximation seems more accurate than for out-of-the-money options, even though the relative difference oscillates around 0.7%. The approximation for out-the-money options seems to be divergent the longer the maturities.

Conclusion

The analysis of time-series of volatility and financial instruments whose underlying is linked to volatility helps us confirm that volatility is rough. The roughness of volatility is modelled via fractional Brownian motion, which covariance structure helps model log-volatility increments. Modelling log-variance with fractional Brownian motion has allowed to forecast volatility and to price vanilla instruments along with exotic options using the rough Bergomi model.

In the rBergomi model, the calibration to volatility surfaces, although still with a relatively significant time of execution, enables to choose parameters for different maturities, whether short (one-week) or long (two-year). Besides, the low number of parameters (only three) makes the model more usable in practice. Volatility skew is an important matter as well as it can allow to choose a certain function to simulate volatility as we have begun to see.

Last but not least, rBergomi is used to model dynamics of VIX derivatives, such as Futures and options and different techniques allow to generate prices for these contracts.

A Appendix

A.1 Proof 1: VIX formula

Proof. It has been shown that, with $v = \sigma^2$,

$$VIX_T^2 = \frac{1}{\Delta} \int_T^{T+\Delta} \mathbb{E}^{\mathbb{Q}}\left[v_t | \mathcal{F}_T\right] dt.$$

Using the representation of instantaneous variance in the rBergomi model, i.e.

$$v_t = \xi_0(t)\mathcal{E}\left(2\nu C_H \int_0^t \frac{1}{(t-u)^{1/2-H}} dZ_u^{\mathbb{Q}}\right)$$

$$= \xi_0(t)\eta_T(t)\exp\left[2\nu C_H \mathcal{I}_T^t - \frac{\nu^2 C_H^2 t^{2H}}{H}\right].$$

where

$$\mathcal{I}_T^t = \int_T^t \frac{1}{(t-u)^{1/2-H}} dZ_u^{\mathbb{Q}}$$

Since $\eta_T(t)$ is $\mathcal{F}_T$-measurable and $\xi_0(t)$ is $\mathcal{F}_0$-measurable, VIX is expressed as

$$VIX_T^2 = \frac{1}{\Delta} \int_T^{T+\Delta} \xi_0(t)\eta_T(t)\mathbb{E}^{\mathbb{Q}}\left[\exp\left(2\nu C_H \mathcal{I}_T^t - \frac{\nu^2 C_H^2 t^{2H}}{H}\right)\bigg|\mathcal{F}_T\right]$$

As $\int_T^t \frac{1}{(t-u)^{1/2-H}} dZ_u^{\mathbb{Q}}$ is centered Gaussian of variance $2\frac{\nu^2 C_H^2}{H}(t-T)^{2H}$, independent of $\mathcal{F}_T$,

$$\mathbb{E}^{\mathbb{Q}}\left[\exp\left(2\nu C_H \mathcal{I}_T^t\right)\right] = \exp\left(\frac{\nu^2 C_H^2}{H}(t-T)^{2H}\right).$$

Hence

$$VIX_T^2 = \frac{1}{\Delta} \int_T^{T+\Delta} \xi_0(t)\eta_T(t)\exp\left[\frac{\nu^2 C_H^2}{H}\left((t-T)^{2H} - t^{2H}\right)\right] dt.$$

$\square$

References

[1] O.E. Barndorff-Nielsen and J. Schmiegel. Brownian semistationary processes and volatility/intermittency. *Advanced Financial Modelling*, de Gruyter, pp. 1-26, 2009.

[2] C. Bayer, P. Friz, J. Gatheral. Pricing under rough volatility. *Quantitative Finance*, pp. 1-18, 2015.

[3] M. Bennedsen, A. Lunde and M. S. Pakkanen. Hybrid scheme for Brownian semistationary process. Working paper, available at arXiv:1507.03004, 2015.

[4] L. Bergomi. Smile dynamics II. *Risk*, 10, pp. 67-73, 2005.

[5] L. Bergomi. Stochastic Volatility Modeling. 2015.

[6] F. Black and M. Scholes. The Pricing of Options and Corporate Liabilities. *Journal of Political Economy, Vol. 81, No. 3*, pp. 637-654, 1973.

[7] P. Carr and D. Madan. Towards a theory of volatility trading. *Risk Publications*, pp. 417-427, 1998.

[8] F. Comte and E. Renault. Long memory in continuous-time stochastic volatility model. *Mathematical Finance*, 8(4): 291-323, 1998.

[9] D. Dufresne. The log-normal approximation in financial and other computations. *Adv. in App. Prob, 36*, pp. 747-773, 2004.

[10] J. Gatheral. A parsimonious arbitrage-free implied volatility parameterization with application to the valuation of volatility derivatives. *Presentation at Global Derivatives*, 2004.

[11] J. Gatheral and A. Jacquier. Arbitrage-free SVI volatility surfaces. *Quantitative Finance*, 14(1): 59–71, 2014.

[12] J. Gatheral, T. Jaisson and M. Rosenbaum. Volatility is rough. Available at arXiv:1410.3394, 2014.

[13] P.S. Hagan, D. Kumar, A. Lesniewski and D.E. Woodward. Managing smile risk. *Wilmott Magazine*, pp. 84-108, 2002.

[14] S. Heston. A closed-form solution for options with stochastic volatility with applications to bond and currency options. *The Review of Financial Studies, Vol. 6, No, 2*, pp. 327-342, 1993.

[15] B. Horvath, A. Jacquier and A. Muguruza. Functional Central Limit Theorems for Rough Volatility. Available at arXiv:1711.03078, 2017.

[16] J. Hull and A. White. Pricing interest-rate derivative securities, *The Review of Financial Studies, Vol. 3, No. 4*, pp. 573–592, 1990.

[17] A. Jacquier, C. Martini and A. Muguruza. On VIX Futures in the rough Bergomi model. Available at arXiv:1701.04260, 2017.

[18] D. Kraft. A software package for sequential quadratic programming. *Tech. Rep. DFVLR-FB, Vol. 88-28*, DLR German Aerospace Center, Institute for Flight Mechanics, Koln, Germany, 1988.

[19] B. Mandelbrot and J. Van Ness. Fractional Brownian motions, fractional noises and applications. *SIAM Review, Vol. 10, No. 4*, pp. 422-437, Oct. 1968.

[20] R. McCrickerd. rBergomi simulation and turbocharged pricing. GitHub repository github.com/ryanmccrickerd, 2017.

[21] C. J. Nuzman and V. H. Poor. Linear estimation of self-similar processes via Lamperti's transformation. *Journal of Applied Probability, Vol. 37, No. 2*, pp. 429-452, 2000.